

TDP-43 Modulation by Tau-Tubulin Kinase 1 Inhibitors: A New Avenue for Future Amyotrophic Lateral Sclerosis Therapy

Vanesa Nozal, Loreto Martínez-González, Marta Gomez-Almeria, Claudia Gonzalo-Consuegra, Paula Santana, Apirat Chaikuad, Eva Pérez-Cuevas, Stefan Knapp, Daniel Lietha, David Ramírez, Sabrina Petralla, Barbara Monti, Carmen Gil, Angeles Martín-Requero, Valle Palomo, Eva de Lago, and Ana Martinez*



Cite This: <https://doi.org/10.1021/acs.jmedchem.1c01942>



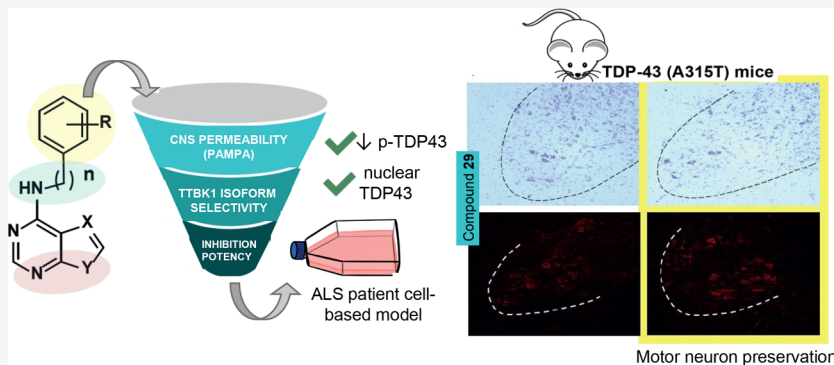
Read Online

ACCESS |

Metrics & More

Article Recommendations

Supporting Information



ABSTRACT: Amyotrophic lateral sclerosis (ALS) is a fatal neurodegenerative disease without any effective treatment. Protein TDP-43 is a pathological hallmark of ALS in both sporadic and familiar patients. Post-translational modifications of TDP-43 promote its aggregation in the cytoplasm. Tau-Tubulin kinase (TTBK1) phosphorylates TDP-43 in cellular and animal models; thus, TTBK1 inhibitors emerge as a promising therapeutic strategy for ALS. The design, synthesis, biological evaluation, kinase–ligand complex structure determination, and molecular modeling studies confirmed novel pyrrolopyrimidine derivatives as valuable inhibitors for further development. Moreover, compound 29 revealed good brain penetration *in vivo* and was able to reduce TDP-43 phosphorylation not only in cell cultures but also in the spinal cord of transgenic TDP-43 mice. A shift to M2 anti-inflammatory microglia was also demonstrated *in vivo*. Both these activities led to motor neuron preservation in mice, proposing pyrrolopyrimidine 29 as a valuable lead compound for future ALS therapy.

1. INTRODUCTION

Amyotrophic lateral sclerosis (ALS) is a fatal and rare neurodegenerative disease that affects motoneurons, causing the death of the patients within three to five years after disease onset due to cardiorespiratory failure. Despite this fatal outcome, disease-modifying agents have not been discovered, and current therapeutic options only expand the lifespan of the patients up to several months. Multiple pathological mechanisms have been described to occur in the affected motor neurons, among which are deposits of TAR DNA binding protein of 43 kDa (TDP-43), which are present in the 97% of the patients independent from their etiological origin, sporadic or familial.¹ TDP-43 is a highly conserved nuclear protein that plays many different roles in RNA metabolism such as transcription, splicing, transport, stability through recruitment into stress granules, and microRNA biosynthesis.² In ALS and other TDP-43 pathologies such as the rare Alexander's disease, frontotemporal dementia (FTD-TDP), or the prevalent limbic-

predominant age-related TDP-43 encephalopathy (LATE), nuclear localization of TDP-43 is lost.³ Elevated levels of this protein are present in the cytoplasm of ALS patients, which are affected by different post-translational modifications thought to impede the return of the protein to the nucleus.⁴ Among them, aberrant hyperphosphorylation is the most relevant one in TDP-43 inclusions.⁵ Therefore, the recovery of TDP-43 homeostasis is an emergent therapeutic approach for the discovery of new drugs for ALS and other severe diseases.⁶

Only few kinases have been described to participate directly or indirectly in TDP-43 phosphorylation, including glycogen

Special Issue: New Horizons in Drug Discovery - Understanding and Advancing Kinase Inhibitors

Received: November 12, 2021

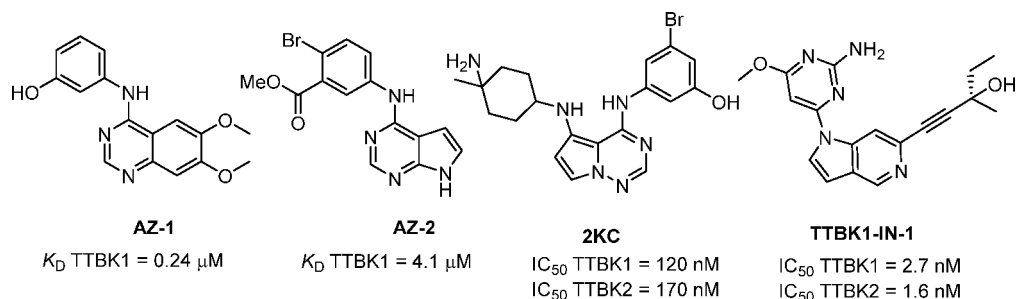


Figure 1. Chemical structure of the few described TTBK1 inhibitors and their reported K_D or IC_{50} values.

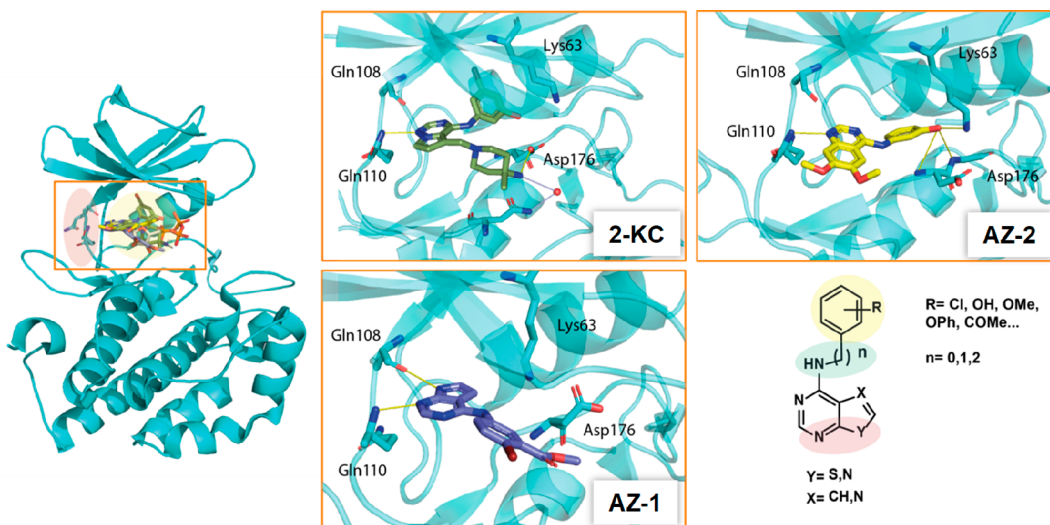


Figure 2. Crystal structure of kinase domain of TTBK1 with compounds AZ-1, AZ-2, and 2KC (PDB IDs 4BTM, 4BTK, and 4NFN, respectively) that led to the design of the new TTBK1 inhibitors.

synthase kinase 3 β (GSK3 β),⁷ casein kinase 1 (CK1),⁸ cell division cycle kinase 7 (CDC7),⁹ mitogen-activated protein kinases (MAPK/ERK),¹⁰ and Tau-tubulin kinases (TTBK1 and TTBK2).¹¹ Consequently, inhibitors of these proteins have thus been considered as an emerging therapeutic option.¹² Several inhibitors of GSK3 β , CK1, and CDC7 have been described and tested in ALS models.^{13–15} In addition, despite the fact that inhibitors for TTBK1 and TTBK2 were recently disclosed,¹⁶ their role in TDP-43-pathies has not been explored so far.

TTBKs belong to the superfamily of CK1, which contains two isoforms in human: TTBK1 and TTBK2 with different expression patterns throughout the body and different physiological roles. TTBK2 expression is ubiquitous, and mutations in TTBK2 gene trigger spinocerebellar ataxia 11 (SCA11) since the protein is involved in ciliogenesis. Furthermore, mice that presented truncated TTBK2 showed embryonic lethality with a strong neural tube and sonic hedgehog signaling defects. These data emphasize the relevance of this kinase in modulating physiological pathways and the challenge of targeting it by small molecules without toxic events.^{17,18} On the other hand, TTBK1 is specifically expressed in the central nervous system (CNS) and is linked to neuronal pathological roles.¹⁹ TTBK1 was described for the first time in 2006 as a kinase responsible for the phosphorylation and aggregation of Tau.²⁰ Since then, multiple studies have demonstrated the role of TTBK1 in the modulation of τ linked with Alzheimer's disease (AD), as it is the main kinase responsible for the phosphorylation of

Ser422, a key epitope in the early formation of fibrils prior to neurofibrillary tangles (NFT).^{21,22} Regarding TDP-43 pathologies, Liachko et al. established a relevant role of TTBK1 in TDP-43 phosphorylation, demonstrating the ability of the kinase to phosphorylate TDP-43 Ser409 and Ser410 both *in vitro* and *in vivo*. siRNA treatment in a *Caenorhabditis elegans* model resulted in different outcomes for the two isoforms, where only the depletion of TTBK1 by siRNA resulted in the significantly reduced phosphorylation of TDP-43.¹¹ Thus, TTBK1 has emerged as a potential drug target for neurodegenerative diseases where the pathology of TDP-43 plays a key role, and its inhibitors may play a crucial role in several unmet diseases such as ALS, LATE, and FTD.²³

Only few small molecules have been reported to inhibit TTBK1 (Figure 1). Two chemical diverse compounds, namely 3-[[(6,7-dimethoxyquinazolin-4-yl)amino]phenol (AZ-1) and methyl 2-bromo-5-(7H-pyrrolo[2,3-*d*]pyrimidin-4-ylamino)-benzoate (AZ-2), have been identified as binders of TTBK1 using surface plasmon resonance.²⁴ Furthermore, the crystal structures of both compounds in complex with the kinase domain of TTBK1 have been determined, but neither the IC_{50} values for TTBK1 and TTBK2 nor their selectivity against other kinases has been described aside from their K_D . The heterocyclic compound 3-{5-[[(4-amino-4-methylpiperidin-1-yl)methyl]pyrrolo[2,1-*f*][1,2,4]triazin-4-yl]amino}-5-bromophenol (2KC) with equipotent IC_{50} values for TTBK1 and TTBK2 (120 and 170 nM, respectively) has been also described in crystallographic complex with the kinase domain of TTBK1.²⁵ However, neither the kinase selectivity profile of

these three compounds nor their behavior in cellular models has been reported. During the preparation of this manuscript, the first brain-penetrant TTBK1 inhibitors have been reported, including the azaindazole **TTBK1-IN-1**, and target engagement and a decrease of Tau-phosphorylation *in vivo* have been shown despite their lack of selectivity for TTBK2.^{16,26} These data corroborate the therapeutic relevance of TTBK1 inhibitors for tauopathies and especially for Alzheimer's disease.

In this work we describe the design, synthesis, and optimization of new TTBK1 isoform-selective inhibitors for the treatment of TDP-43 proteinopathies. A family of more than 60 heterocyclic compounds was synthesized, and their inhibition of TTBK1 and TTBK2 was tested *in vitro*. Their selectivity for the TBK1 isoform, permeability through the blood–brain barrier, crystal structures of the kinase–inhibitor complexes with TTBK1 and TTBK2, molecular dynamics, and cellular activity in ALS disease models are presented. Finally, one of the most promising candidates was studied in a TDP-43^{A315T} transgenic mouse model. Our results confirmed the therapeutic potential of TTBK1 for ALS and other TDP-43-pathologies, and the compounds reported represent promising lead structures for the treatment of these diseases.

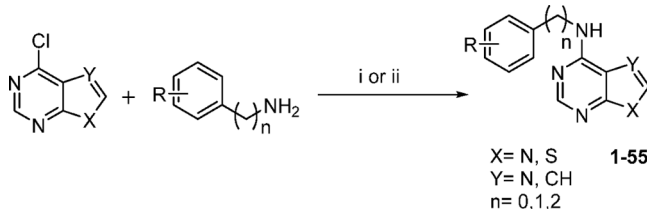
2. RESULTS AND DISCUSSION

2.1. Design, Synthesis, and Enzymatic Evaluation of TTBK Inhibitors. When this medicinal chemistry program began few years ago, the kinase domain of TTBK1 with ATP (PDB ID 4BTJ) together with three small molecules that bind to the adenine binding pocket (PDB IDs 4BTM, 4BTK, and 4NFN) were available in the Protein Data Bank.^{24,25} Until very recently, the crystal structure of the catalytic domain of TTBK2 had not been determined.^{22,27} This body of structural information was considered a starting point for our drug design program. As such, the design of new compounds aimed to study the importance of two hydrogen bonds with Gln108 and Gln110 located in the hinge region and explore the druggability of the hydrophobic pocket around Asp176 and the catalytic Lys63 (Figure 2).

Hence, we chose a [6 + 5] heterocycle, which is considered a privileged scaffold for protein kinase inhibitors,²⁸ as a central core, varying the nature of the five-membered ring to explore the importance of a hydrogen-donor atom for the interaction with Gln110 and Gln108. Furthermore, we linked directly to this heterocycle a phenyl ring with different substituents, including halogens and hydrogen-bond donors and acceptors, in different positions. The introduced phenyl ring would presumably establish interactions in the hydrophobic pocket (yellow area in Figure 2). The nature and length of the linker were also varied to explore this hydrophobic region (green area in Figure 2).

The synthesis of the compounds was easily realized by implementing a one-step reaction with indium trichloride as a Lewis acid to facilitate the aromatic nucleophilic substitution of π -deficient heterocycles (Scheme 1).²⁹ In cases where a halogen atom was a substituent in the phenyl ring, we discarded the use of InCl_3 to avoid the polymerization of the building blocks. Synthesis of these compounds was achieved using THF as the solvent under microwave irradiation. A first family of 27 compounds (**1–27**) was synthesized following this methodology with moderate to very good yields (Scheme 1 and Table 1). Their chemical structure was confirmed by

Scheme 1^a



^a(i) InCl_3 (0.1 equiv), MW, MeCN, 100 °C; (ii) MW, THF, 100 °C (See Table 1 and 2 for the description of R).

NMR (¹H and ¹³C NMR) and other analytical methods as detailed in the Experimental section.

The inhibitory activities of the newly prepared compounds against TTBK isoforms 1 and 2 were evaluated in the Medical Research Council (MRC) Phosphorylation Unit (University of Dundee). Data are shown in Table 1. Initially, the compounds were tested at a fixed concentration of 10 μM , and when the inhibition was larger than 50%, a dose-response analysis was conducted to determine IC_{50} values. Overall, the tested compounds showed TTBK1 inhibition in the low micromolar range and were either equipotent at inhibiting TTBK2 or showed activity approximately up to one order of magnitude lower. These results and the calculation of the “TTBK1 selectivity index” defined as $\text{IC}_{50(\text{TTBK1})}/\text{IC}_{50(\text{TTBK2})}$ allowed us to establish limited structure–activity relationships to improve the TTBK1 activity.

Considering the main heterocycle, pyrrolopyrimidine-derived compounds were more active than their purine derivative analogues (see compounds **1–4** versus **7–10**) that lacked kinase inhibitory activity. The thienopyrimidine-derived compounds **5** and **6** also resulted in inactive compounds. Altogether, these results highlighted the importance of the presence of a hydrogen-donor atom at position 7 in the five membered-ring and motivated us to choose the pyrrolopyrimidine moiety as the main scaffolding heterocycle.

The length of the connector of the phenyl moiety attached at the exocyclic amino group was also crucial for TTBK1 inhibition. Thus, the presence of only one methylene group in the linker negatively affected the activity and resulted in inactive compounds (**11** and **13**). Additionally, the introduction of two methylene groups resulted in less potent compounds than those with the phenyl ring directly attached to the amine (derivatives **8** versus **14** and **10** versus **12**).

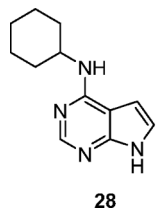
Moreover, the position of substituents in the phenyl ring affects the potency of the inhibitors, highlighting *para*-substitution as the more favorable modification to increase TTBK1 inhibition (i.e., **10** > **15** > **16** or **8** > **7** > **17**). Interestingly, the best IC_{50} value (in the low micromolar range) was obtained with a compound bearing a second aromatic ring in the *para*-position of the aniline ring (compound **27**).

Finally, we synthesized compound **28** (Figure 3) where the phenyl ring was replaced by the saturated cyclohexyl moiety. The lack of TTBK1 inhibition highlighted the importance of this aromatic ring for compound activity.

The discovery of **27** motivated us to further exploit this family of compounds. Consequently, we designed a second subfamily of ligands harboring two aromatic rings with different substituents and linkers connected to a pyrrolopyrimidine heterocycle. These compounds (**29–54**) were prepared following the reaction conditions of Scheme 1 and

Table 1. Chemical Structure, Yield, and Enzymatic Inhibition of the Synthesized Compounds 1–27 against TTBK1 and TTBK2

compound	Y	X	n	R	yield (%)	TTBK1 IC ₅₀ (μ M) or %inh@10 μ M	TTBK2 IC ₅₀ (μ M) or %inh@10 μ M	selectivity index A/B
1	N	NH	0	3-OH	29	9.15 μ M	13%@10 μ M	0.22
2	N	NH	0	4-OH	20	3%@10 μ M	1%@10 μ M	
3	N	NH	0	4-morpholine	70	25%@10 μ M	12%@10 μ M	
4	N	NH	0	4-Cl	75	8%@10 μ M	1%@10 μ M	
5	CH	S	0	4-Cl	50	20%@10 μ M		
6	CH	S	0	H	70	17%@10 μ M		
7	CH	NH	0	3-OH	87	6.10 μ M	6.70 μ M	0.90
8	CH	NH	0	4-OH	38	3.00 μ M	7.40 μ M	0.45
9	CH	NH	0	4-morpholine	24	4.90 μ M	15.70 μ M	0.30
10	CH	NH	0	4-Cl	92	3.20 μ M	20.30 μ M	0.15
11	CH	NH	1	4-Cl	55	32%@10 μ M	10%@10 μ M	
12	CH	NH	2	4-Cl	25	18.20 μ M	86.00 μ M	
13	CH	NH	1	4-OH	14	23%@10 μ M	10%@10 μ M	
14	CH	NH	2	4-OH	23	12.80 μ M	37.70 μ M	0.33
15	CH	NH	0	3-Cl	49	15.20 μ M	13.90 μ M	1.09
16	CH	NH	0	2-Cl	69	21.80 μ M	42.10 μ M	0.51
17	CH	NH	0	2-OH	20	14%@10 μ M	1%@10 μ M	
18	CH	NH	0	[b]cyclohexyl	23	23%@10 μ M	10%@10 μ M	
19	CH	NH	0	[b]1,3dioxole	15	1.58 μ M	7.58 μ M	0.21
20	CH	NH	0	4-COMe	25	4.30 μ M	9.30 μ M	0.46
21	CH	NH	0	3-morpholine	58	4.70 μ M	5.70 μ M	0.82
22	CH	NH	0	H	64	0.79 μ M	1.68 μ M	0.47
23	CH	NH	0	4-OMe	74	0.52 μ M	1.32 μ M	0.39
24	CH	NH	0	4-OCF ₃	92	1.00 μ M	8.80 μ M	0.11
25	CH	NH	0	4-OiPr	66	1.50 μ M	8.40 μ M	0.17
26	CH	NH	0	4-OEt	20	2.30 μ M	13.70 μ M	0.16
27	CH	NH	0	4-OPh	53	0.39 μ M	0.85 μ M	0.45



Yield (%)	TTBK1		TTBK2	
	%inh@10 μ M	%inh@10 μ M	%inh@10 μ M	%inh@10 μ M
26%	3 %		15%	

Figure 3. Chemical structure, yield, and inhibition of TTBK1 and TTBK2 of compound 28.

were enzymatically evaluated against TTBK1 and TTBK2 as outlined before. Data are summarized in Table 2, revealing more potent TTBK1 inhibitors in this second set of compounds with IC₅₀ values in submicromolar range. Furthermore, and although selectivity in these two isoenzymes is a great challenge, compounds 29 and 39 may be considered as TTBK1-selective inhibitors as a factor of 10 is present in their IC₅₀ values.

In light of these biological activities, some conclusions may be drawn. The preferred connector between the two phenyl rings is the ether one (−O−), followed by the thioether (−S−) and the carbonyl (−CO−) moieties. In that sense, compounds 52 and 53 with a carbonyl group linking the phenyl groups resulted in less potency than their counterparts 27 and 30,

respectively, which have an ether group as linker. At the same time, derivatives 35 and 36 were slightly more potent or equipotent compared to their thio-analogs 49 and 50, respectively.

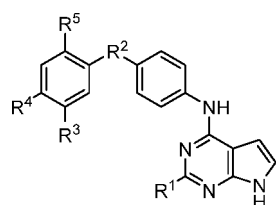
The introduction of an amino group in position 2 of the pyrrolopyrimidine core led to compounds potent against TTBK1 but less selective (29, 33, 39, and 40 versus 45–48, respectively).

Regarding the substitution in the second phenyl ring, a combination of steric and electrostatic factors may influence the inhibition of the two isoforms. Thus, the most selective TTBK1 inhibitors were derivatives 29, 33, 39, and 40 with chlorine or trifluoromethyl- substituents in *meta*- and *para*-positions, with compound 29 being identified as the most potent and selective TTBK1 inhibitor.

Finally, introduction of the π-deficient pyridine heterocycle (compound 55, Figure 4) tends to increase the selectivity in comparison to its analog 27.

A third subfamily of compounds was synthesized by exploring modifications in the second aromatic group. In this series, we prepared a set of different organic azides (56–60) and the alkyne 61. Additionally, using the cooper(I)-catalyzed alkyne–azide cycloaddition (CuAAC) methodology,³⁰ new ligands bearing a triazole ring (62–67) were synthesized with good yields (Scheme 2, Table 3).

Table 2. Chemical Structure, Yield, And Biological Inhibition of the Synthesized Compounds 29–55 against TTBK1 and TTBK2



compound	R ¹	R ²	R ³	R ⁴	R ⁵	yield (%)	TTBK1 IC ₅₀ (μ M) or %inh@ 10 μ M	TTBK2 IC ₅₀ (μ M) or %inh@ 10 μ M	selectivity index A/B
29	H	—O—	H	Cl	H	62	0.24 μ M	4.22 μ M	0.05
30	H	—O—	H	F	H	40	0.77 μ M	3.02 μ M	0.25
31	H	—O—	H	CN	H	6	0.44 μ M	2.14 μ M	0.20
32	H	—O—	H	OMe	H	63	0.54 μ M	0.97 μ M	0.55
33	H	—O—	H	CF ₃	H	74	5.03 μ M	5%@10 μ M	0.06
34	H	—O—	H	Br	H	83	0.75 μ M	1.21 μ M	0.61
35	H	—O—	H	NO ₂	H	83	0.42 μ M	1.24 μ M	0.33
36	H	—O—	H	NH ₂	H	9	0.52 μ M	4.90 μ M	0.10
37	H	—O—	H	Me	H	57	1.02 μ M	8.79 μ M	0.11
38	H	—O—	Me	H	H	80	2.20 μ M	6.40 μ M	0.34
39	H	—O—	Cl	H	H	62	1.55 μ M	1%@10 μ M	0.02
40	H	—O—	CF ₃	H	H	78	5.61 μ M	1%@10 μ M	0.06
41	H	—O—	OMe	H	H	33	0.84 μ M	6.79 μ M	0.12
42	H	—O—	H	H	Cl	79	0.53 μ M	0.49 μ M	1.08
43	H	—O—	H	H	OMe	64	3.56 μ M	9.54 μ M	0.37
44	H	—O—	H	Cl	Cl	63	2.30 μ M	5.72 μ M	0.40
45	NH ₂	—O—	H	Cl	H	70	0.45 μ M	2.70 μ M	0.16
46	NH ₂	—O—	H	CF ₃	H	77	0.58 μ M	4.49 μ M	0.13
47	NH ₂	—O—	Cl	H	H	16	0.37 μ M	3.05 μ M	0.12
48	NH ₂	—O—	CF ₃	H	H	45	1.32 μ M	3.90 μ M	0.33
49	H	—S—	H	NO ₂	H	42	2.72 μ M	22.72 μ M	0.11
50	H	—S—	H	NH ₂	H	69	0.65 μ M	4.94 μ M	0.13
51	H	—OCH ₂ —	H	H	H	28	0.75 μ M	1.21 μ M	0.61
52	H	—CO—	H	H	H	97	1.71 μ M	11.92 μ M	0.14
53	H	—CO—	H	F	H	19	1.50 μ M	5.4 μ M	0.27
54	H	—CO—	Cl	Cl	H	35	9%@10 μ M		

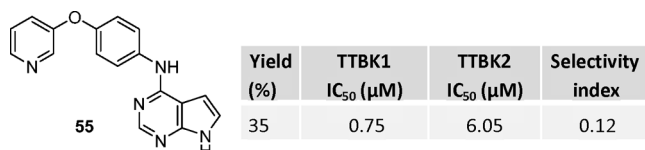


Figure 4. Chemical structure, yield, and inhibition of TTBK1 and TTBK2 of compound 55.

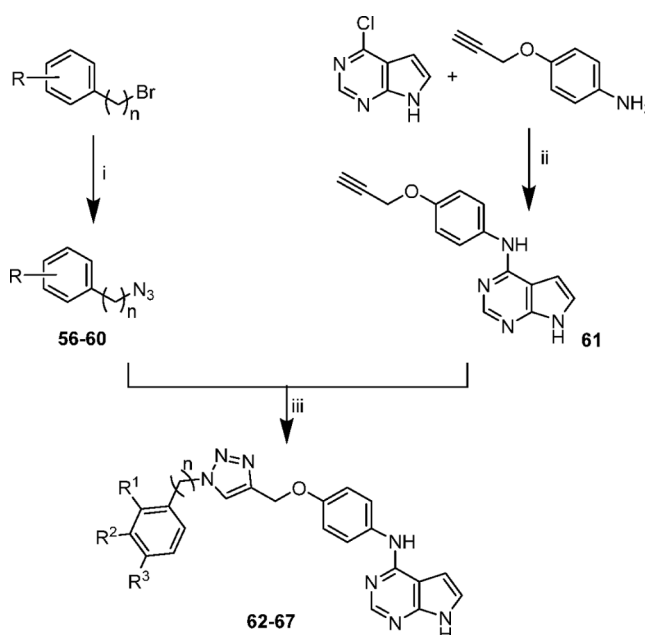
Data on this series are summarized in Table 3. In general, compounds containing a triazole ring resulted in moderately selective TTBK1 inhibitors.

2.2. Elucidation of Ligand–kinase Binding Modes. Since the homology of kinase domains of the two isoforms is high with 88% identity and 96% similarity, we aimed to crystallize different protein–ligand complexes and computationally study the binding modes of the compounds with the different kinases to explain the experimentally observed selectivity of the synthesized inhibitors. For this purpose, we crystallized the kinase domains of TTBK1 (13–313) and TTBK2 (6–299) (see the Experimental section for detailed information) with different compounds, including 23, 27, 29, 32, and 42 (Figures S1 and 5 and Table S1). Among these, the derivatives 29 and 42 (Figure 5) were of particular interest as they had different affinities for TTBK1 and TTBK2.

The structures confirmed that all compounds bound to the ATP pocket, forming canonical hydrogen bonds with the hinge region residues Gln108 and Gln110 of TTBK1 and residues Gln95 and Gln97 of TTBK2. Only in TTBK2 was a water-mediated hydrogen bond was formed between the nitrogen in the position 1 of the pyrrolopyrimidine ring, Gly98, and Asn100. Crystal structures of TTBK1 with derivatives 29 and 42 were highly similar (Figure 5a and c). However, despite the initial hypothesis of an interaction with the catalytic lysine located in the hydrophobic pocket, all the compounds displayed their aromatic substituents toward the front pocket. In this binding mode, the interaction between compound 29 and Arg119 in TTBK1, which was not observed in the complex with 42, seemed to be important for the potency of the compound for TTBK1.

A comparison of the structures of compound 42 bound to both TTBK isoenzymes revealed some interesting points. First, the glycine-rich loop was displaced up to 5.5 Å between the two isoforms, which may also be attributed to crystal packing (Figure 5d). In addition, this inhibitor formed two water-mediated hydrogen bonds with TTBK2 that were absent for TTBK1 (Figure 5e and f).

A conformational change in the N-terminal to the DFG motif appeared to be induced by these pyrrolopyrimidines,

Scheme 2^a

^a(i) NaN₃ (1.5 equiv), DMF, r.t.; (ii) InCl₃ (0.1 equiv), MW, MeCN, 100 °C; (iii) CuSO₄ (0.1 equiv), tris(benzyltriazolylmethyl)amine (0.1 equiv), sodium ascorbate (0.2 equiv), DMF, r.t.

resulting in the flipping of the backbone carbonyl of Leu175 compared to the canonical TTBK1 conformation (Figure 5c). This flip was also observed for TTBK2, allowing the establishment of a water-mediated hydrogen bond between Leu162 and the exocyclic amine group (Figure 5f). The DFG region has been previously demonstrated to exhibit high plasticity, allowing alternative DFG conformations in various kinases.³¹ In addition, such a conformational flip allowed the Leu175 N-terminal to the DFG motif to perform hydrophobic stacking with the pyrrolopyrimidine moiety, a binding mode unique to a subset of kinases that enables an accommodation of kinase inhibitors in the back pocket and may increase inhibitor potency and selectivity.³²

Since all the residues within a 5 Å radius to the ligand were 100% conserved in both isoforms, the observed compound selectivity likely resulted from different dynamic behavior. We therefore performed a molecular mechanics experiment to explain the SAR studies and the selectivity of the compounds toward both isoforms. We use the crystal structures that we obtained as a starting point of these studies. Docking using Glide software and subsequent MM-GBSA calculations were performed to obtain a correlation between calculated free binding energies (ΔG_{bind}) and the observed IC₅₀ values of the active compounds (1–55) against TTBK1. A good correlation

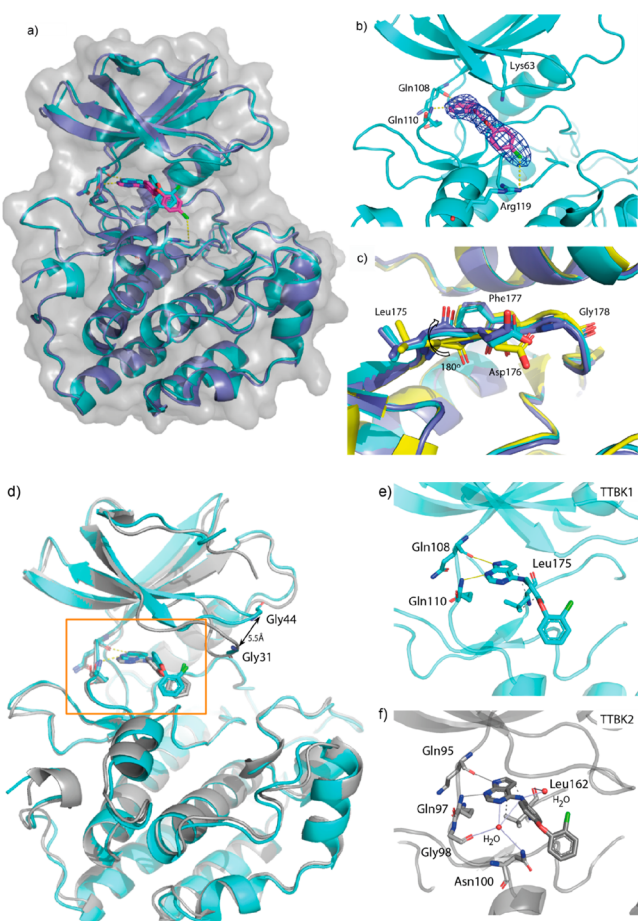


Figure 5. Crystal structures determined by X-ray diffraction of the synthesized compounds with the kinase domain of TTBK. (a) Structure of TTBK1 in complex with 29 (in cyan) and 42 (in purple). (b) Density map and binding mode of 29 with TTBK1 showing the interaction with Arg119. (c) TTBK1 bound to pyrrolopyrimidines displays a flipped conformation of the backbone carbonyl in Leu175 before the DFG (Asp176–Phe177–Gly178) motif compared to ATP-bound TTBK1 (yellow, PDB ID 4BTJ). (d) Superposition of the structures of TTBK1 (cyan) and TTBK2 (gray) bound to compound 42. (e and f) Detailed views of the interactions of compound 42 with TTBK1 and TTBK2, respectively.

coefficient was obtained ($R^2 = 0.7733$), which allowed us to validate these calculations and study the relationship between the predicted free energy values and the experimental biological activity data (Figure S2).

Taking into an account the particular contribution of the energetic terms to the total value of ΔG_{bind} , we observed that Coulomb interactions are important to the increased potency of the compounds and penalized those with lower IC₅₀ values

Table 3. Chemical Structure, Yield, and Biological Inhibition of the Synthesized Compounds 62–67 against TTBK1 and TTBK2

compound	n	R ¹	R ²	R ³	yield (%)	TTBK1 IC ₅₀ (μM) or %inh@10 μM	TTBK2 IC ₅₀ (μM) or %inh@10 μM	selectivity index A/B
62	0	H	H	H	34	29%@10 μM	1%@10 μM	
63	1	H	H	Cl	64	0.61 μM	2.87 μM	0.21
64	1	Cl	H	H	31	0.36 μM	2.75 μM	0.13
65	1	H	Cl	H	33	0.48 μM	2.03 μM	0.24
66	2	H	H	H	64	0.39 μM	2.61 μM	0.15
67	1	H	H	CH ₃	73	0.99 μM	1.75 μM	0.57

together with van der Waals energies, which were also rather low for those compounds with pIC_{50} values below 5.5 (Table S2). These energetic contributions are also important when comparing the free binding energies for selective and nonselective inhibitors, where differences up to 11 kcal/mol are found in the solvation contribution term (Table S3).

To study the dynamics of the binding with the different isoforms, we next performed molecular dynamic (MD) studies with selected compounds. Thus, we studied complexes of both isoforms with inhibitors **29**, **39**, and **42**, which present different patterns of substitution in the second aromatic ring and different selectivity profiles. Crystal structures were used as starting point for complexes **29**–TTBK1, **42**–TTBK1, and **42**–TTBK2. For those cases where the experimental structure was not available, the binding pose obtained by docking studies was the initial point for the MDs.

It was noticed that all the compounds were stable in terms of their catalytic cavity except for compound **39** (Figure 6a). The

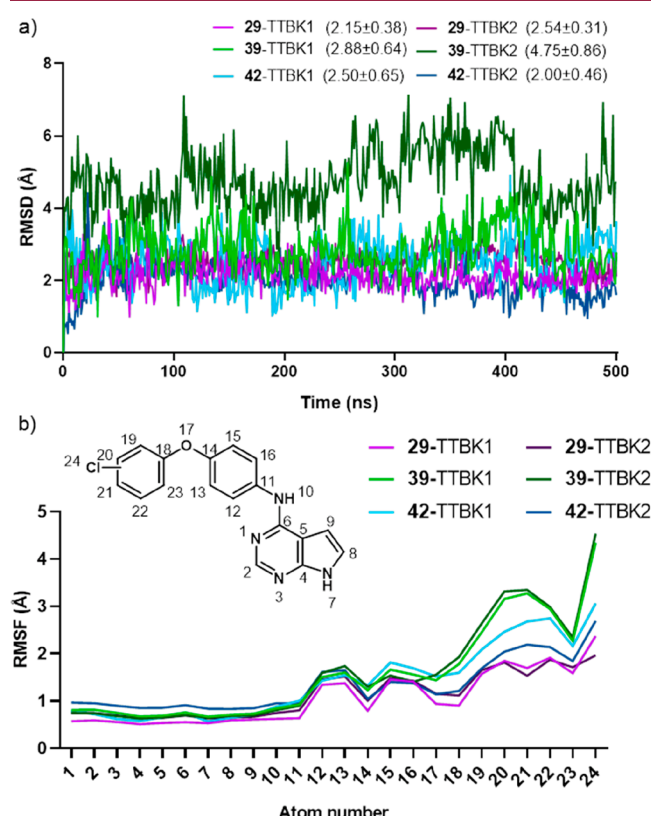


Figure 6. (a) RMSD of the MD trajectories for compounds **29**, **39**, and **42** in TTBK1 and TTBK2. (b) RMSF of the atoms within compounds **29**, **39**, and **42** during the molecular dynamic studies.

root-mean-square deviation (RMSD) value of atomic positions for this compound along the MD study doubles the rest of the compounds, which might be directly related to its low potency for TTBK2 inhibition. It was observed that the stabilities of the modification in compounds within both isoforms were very similar, mainly for pyrrolopyrimidine and phenyl-ether moieties, as it can be deduced from the calculations of the root-mean-square fluctuations (RMSF) of the atoms (Figure 6b). The main difference was the second ring (chlorophenyl moiety), which was much more mobile in compound **39** (RMSF up to 4.5 Å) and reinforced the hypothesis of weak interaction for this molecule.

This compound was only able to establish short hydrophobic interactions; thus, the second aromatic ring was not fixed within the front pocket (Figure S3). The potent compounds **29** and **42** remained tightly positioned toward Arg119, although only compound **29** was able to establish halogen bonds with this residue.

To study carefully how the conformation of the compounds changed during the MD simulations, we clustered every trajectory based on the position of the ligand atoms in each simulation. This allowed us to confirm how stable both compounds **29** and **42** were when interacting with TTBK1 or TTBK2. On the contrary, compound **39** presented different conformations where the chlorophenyl moiety flipped, placing the second aromatic ring in different dispositions within the hydrophobic pocket, impeding a stable conformation of the ring, and reinforcing the idea of weak interactions related to the low potency of the compound (Figure 7).

Finally, since these TTBK1 inhibitors were ATP-competitive, we performed kinase profiling for a set of selected kinases from different families of the human kinome. We screened the TTBK1 inhibitor **29** at a fixed concentration of 10 μM against more than 20 different kinases and calculated the selectivity score (Figure 8). In this case, the S_{35} value, which determines the fraction of kinases that are targeted by the compound **29** beyond 35% of residual activity,³³ was 0.04, showing selectivity over similar kinases.

2.3. Blood–Brain Barrier permeability studies. An important property for a drug candidate or chemical probe that is intended to be used to explore a central nervous system disease, such as ALS, is penetration through the blood–brain barrier (BBB). Using a parallel artificial membrane permeability assay (PAMPA), we determined the predicted brain permeability for all the compounds with an adequate potency (TTBK1 IC_{50} below 2.5 μM). Methodology and individual data are found in the Experimental section and the Supporting Information (Table S4 and Figure S4), while Figure 9 depicts the results of this assay. Compounds **31** and **36** were not soluble under the experimental conditions and could not be tested. In general, all the compounds evaluated under these experimental conditions present permeability values compatible with passive brain penetration, with the exception of four compounds (**23**, **24**, **26**, and **55**) and those containing the triazole ring (**63**–**67**). All these compounds were discarded from subsequent cellular assays.

2.4. TDP-43 Modulation by TTBK1 Inhibitors in Cellular Cultures. The potential decrease of TDP-43 phosphorylation in cellular models was studied only for those brain-permeable TTBK1 inhibitors with a selectivity index regarding this isoform (below 0.25). These criteria resulted in 14 compounds that were tested initially in a human neuroblastoma cell-based model of induced TDP-43 phosphorylation. The SH-SY5Y cell line was exposed to the toxic insult of ethacrynic acid (EA) for 24 h, which increased phosphorylated TDP-43 levels by causing cell death via glutathione depletion.³⁴ In that model, the neuroprotective activity against EA was determined by pretreating the cells with the TTBK1 inhibitors 1 h prior the addition of EA (40 μM). An initial cell viability study at different compound concentrations (5 and 10 μM , Figure S5) ruled out derivatives **30** and **31** from the assay and fixed the study dose at 5 μM . As controls, we used a previously reported TTBK1 inhibitor, methyl 2-bromo-5-(7H-pyrrolo[2,3-d]pyrimidin-4-ylamino) benzoate (AZ-2), which was resynthesized in our laboratory,

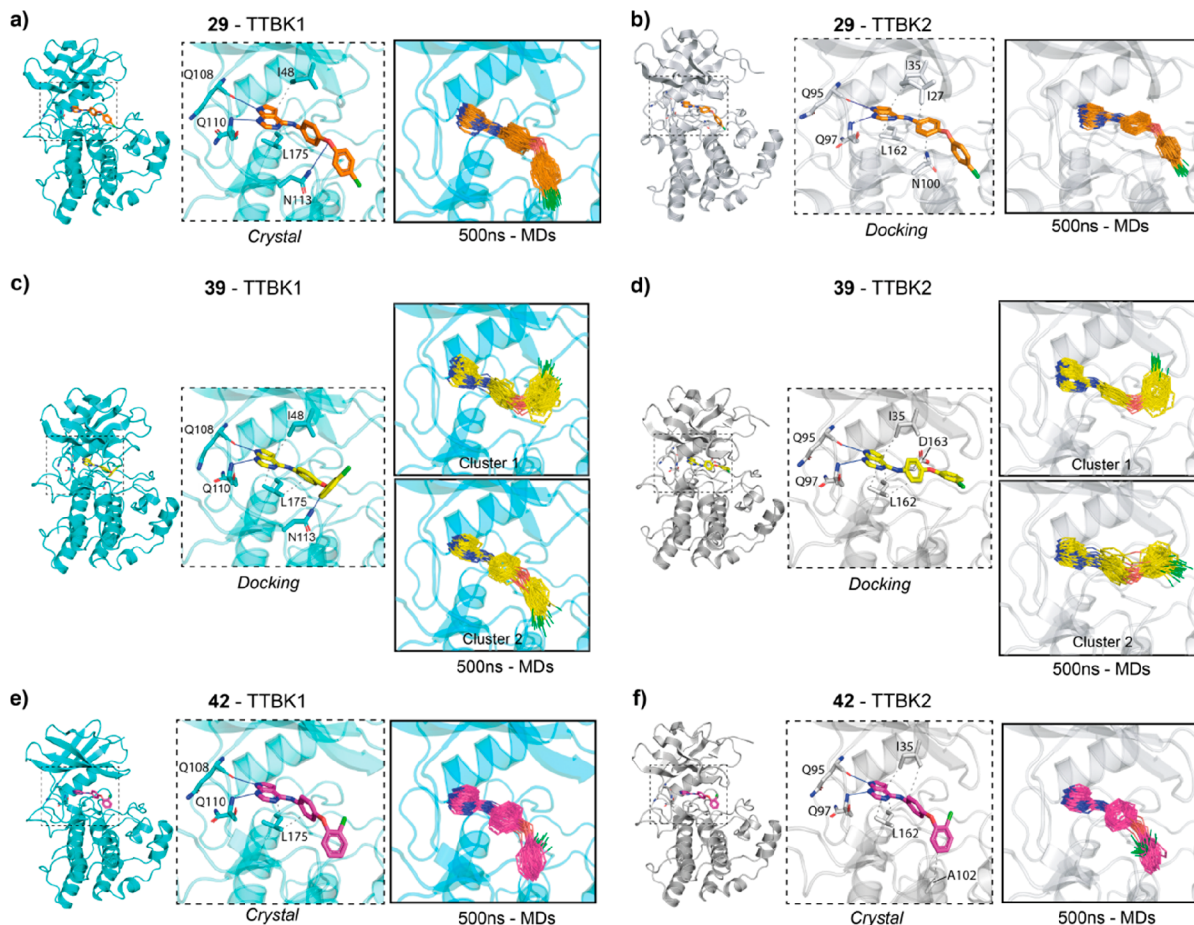


Figure 7. MD simulations of the compounds (a and b) 29, (c and d) 39, and (e and f) 42 with the kinase domains of (a, c, and e) TTBK1 and (b, d, and f) TBK2. The middle panel shows a zoomed-in view with the interactions identified for each compound. Hydrogen bonds and hydrophobic interactions are shown as blue and gray lines, respectively. The right panel shows the most populated clusters obtained from the analysis of the 500 ns MD simulation.

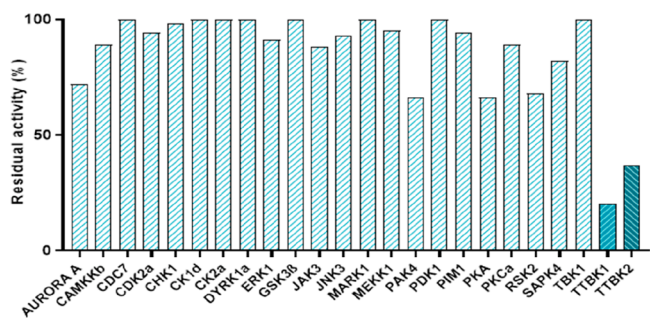


Figure 8. Kinase profiling of the TTBK1 inhibitor derivative 29.

and the known GSK3 inhibitor tideglusib, which showed good results in this cell-based ALS model.¹³ As observed in Figure 10, three compounds (29, 37, and 39) were neuroprotective in this model as they rescued the cells from the death induced by EA (Figure 10a). The next step was to evaluate if this neuroprotective activity was due to the direct modulation of TDP-43. Using Western blot analysis, we showed that the new synthesized compounds were able to reduce TDP-43 hyperphosphorylation to control levels at the important epitopes Ser409 and Ser410; however, the reported TTBK1 inhibitor AZ-2 did not produce such an effect significantly (Figure 10b). We then determined the IC₅₀ of AZ-2 following the same procedure previously described for the pyrrolopyrimidine

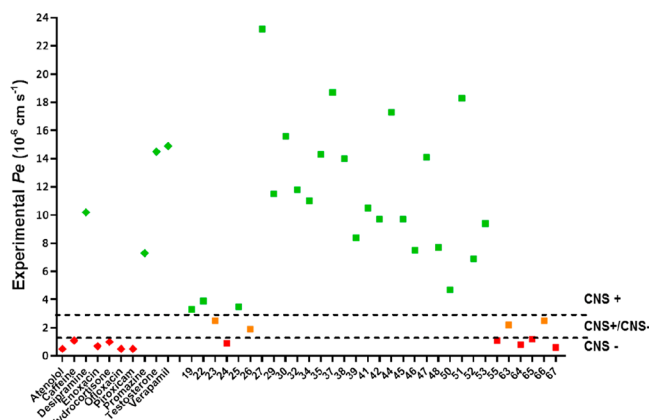


Figure 9. Permeability across the blood–brain barrier of control drugs (diamonds) and TTBK1 inhibitors (squares) was evaluated using the PAMPA methodology (CNS+, permeable, green; CNS-, not permeable, red; CNS \pm , in the shadowed area and either could or could not cross the barrier by passive permeation, orange).

compounds. We determined values much higher and less selective (TTBK1 IC₅₀ = 2.2 μ M and TTBK2 IC₅₀ = 4.2 μ M) than those measured on our derivatives, which may explain the lack of reduction in TDP-43 phosphorylation.

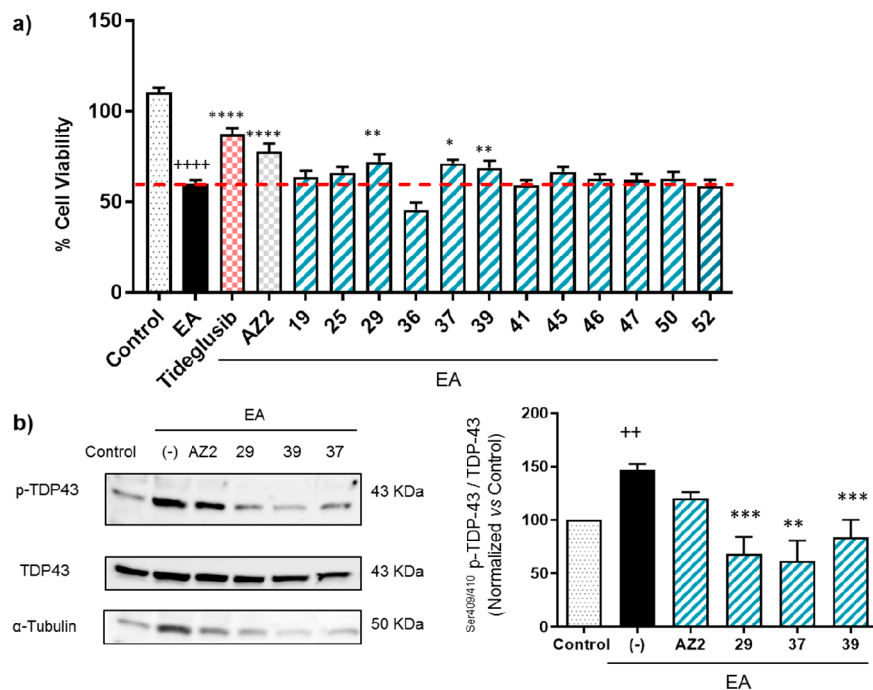


Figure 10. Neuroprotective effect of TTBK1 inhibitors in ethacrynic acid-treated SH-SY5Y neuroblastoma cells. (a) Cell viability measured by MTT assay after being exposed to EA for 24 h in the presence or absence of drug treatment (5 μ M). (b) Representative immunoblot showing TDP-43 phosphorylation levels of SH-SY5Y cells treated with compounds AZ2, 29, 37, and 39 (5 μ M). Each data point represents the mean \pm SEM of three replications in four different experiments (* $p < 0.05$; ** $p < 0.01$, *** $p < 0.001$, **** $p < 0.0001$ significantly different from EA-treated cells; ++ $p < 0.01$, ++++ $p < 0.0001$ significantly different from control cells).

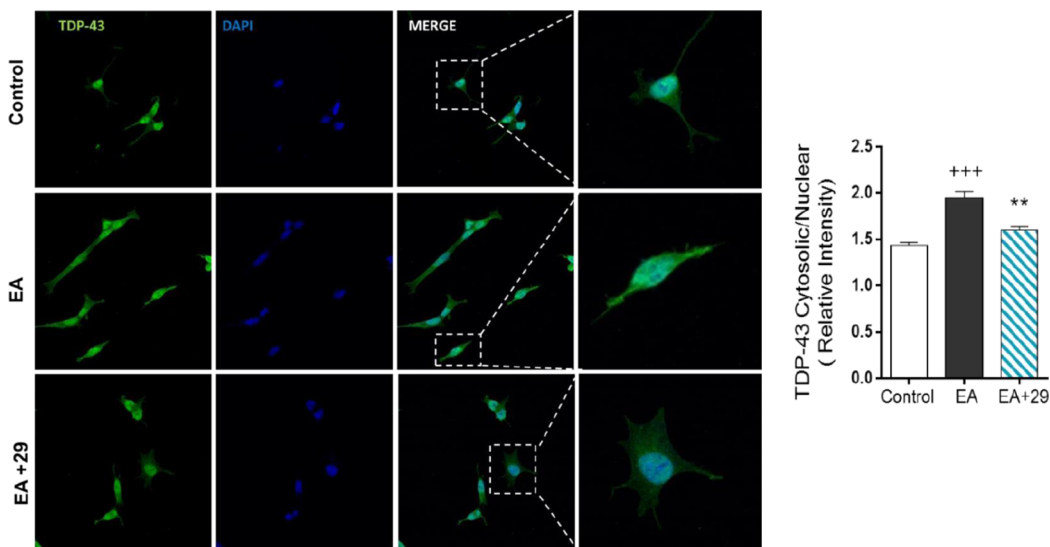


Figure 11. Immunofluorescence analysis of the subcellular localization of TDP-43 in SH-SY5Y cells. Cells were pretreated with compound 29 (5 μ M) and exposed to EA (40 μ M) for 24 h. TDP-43 localization was assessed by confocal laser scanning microscopy. Scale bars are 10 and 20 μ m. Quantification of cytosolic TDP-43 was analyzed in at least 50 different cells from three separate wells ($n = 3$). Data represent the mean \pm SEM (magnification 63 \times) (** $p < 0.005$ significantly different from SH-SY5Y EA-treated cells, +++ $p < 0.001$ significantly different from the control).

We have previously shown that decreased TDP-43 phosphorylation by other kinase inhibitors such as CDC7, CK1, or GSK3 inhibitors restores the physiological nuclear localization of TDP-43.^{13–15} To test if the decrease of TDP-43 phosphorylation using TTBK1 inhibitors also reestablishes the homeostasis of TDP-43 by raising its nuclear localization, we carried out immunofluorescence analyses in EA-treated SH-SY5Y cells. Our findings demonstrated that compound 29 reduced the cytosolic accumulation of TDP-43 in EA-treated

cells, restoring its nuclear localization and therefore the homeostasis of the main pathological hallmark of ALS (Figure 11).

TTBK1 is an enzyme that has been linked to Alzheimer's disease and hyperphosphorylation of Tau, especially at epitope Ser422, which is important for the pretangle formation. Recently, some nonspecific TTBK1 and TTBK2 inhibitors have shown the ability to reduce Tau-phosphorylation both in cellular models and *in vivo*.¹⁶ For this reason, the new synthesized

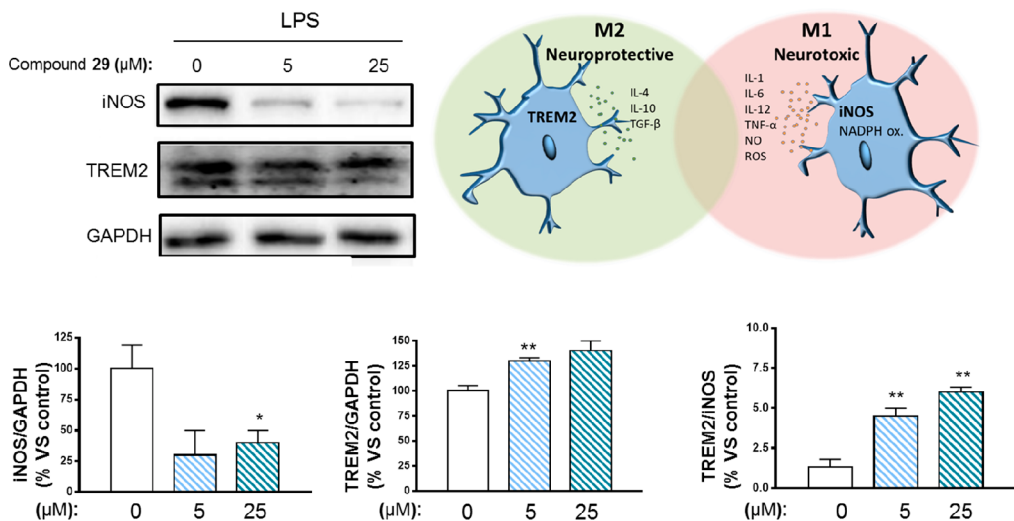


Figure 12. Immunomodulatory effect of compound 29 in primary rat microglial cells. Representative immunoblot showing iNOS and TREM2 protein expression in LPS-treated (100 ng/mL) microglia cells in the presence or absence of compound 29 at increasing concentrations (5 and 25 μ M). GAPDH was used for endogenous normalization. Densitometric data represent the mean \pm SEM of three independent experiments (* $p < 0.05$; ** $p < 0.01$ significantly different from LPS-treated control cells).

Table 4. Pharmacokinetic Parameters of Compound 29 in Plasma and Brain Following a Single Intraperitoneal^a and Oral^b Administration in Male BALB/c Mice

route	dose	matrix	T_{max} (h)	C_{max} (ng/mL)	AUC_{last} (h·ng/mL)	$T_{1/2}$ (h)	brain K_p (AUClast)
i.p.	5 mg/kg	plasma	1.00	1429.08	5958.82	3.75	2.63
		brain ^c	1.00	4174.12	15652.49	3.46	
p.o.	10 mg/kg	plasma	2.00	2265.04	18406.33	3.30	2.67
		brain ^c	2.00	4923.89	49172.57	3.40	

^aDose of 5 mg/kg. ^bDose: of 10 mg/kg. ^cBrain concentration and AUC are expressed as nanograms per gram (ng/g) and hours times nanograms per gram (h·ng/g), respectively.

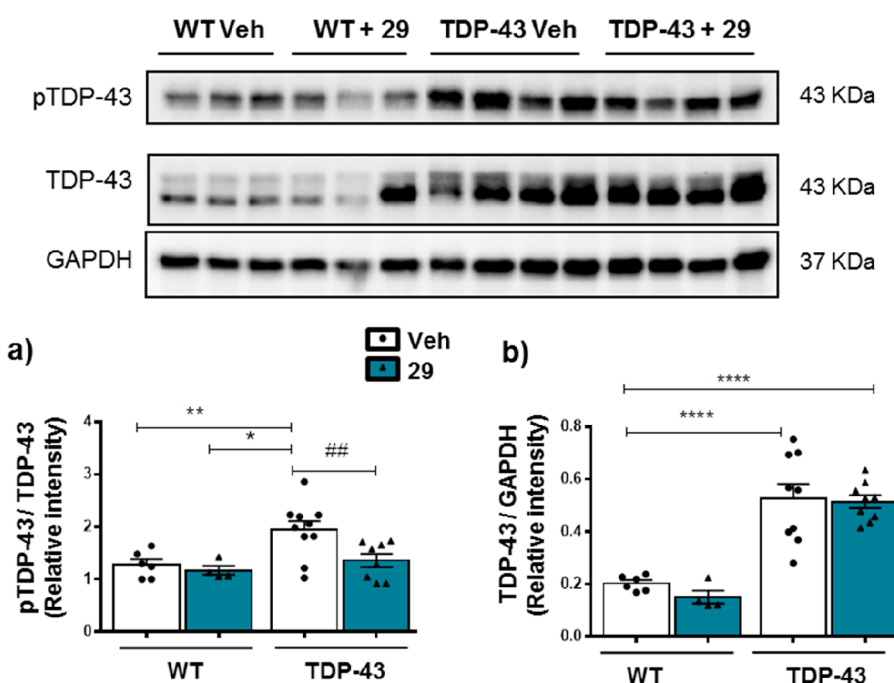


Figure 13. (a) TDP-43 phosphorylated and (b) total TDP-43 levels in the spinal cord of transgenic TDP-43 and wild-type mice treated with compound 29 or the vehicle. Representative immunoblots are shown. Data represent the mean \pm SEM of different observations. Data were assessed by one-way ANOVA, followed by the Bonferroni test (* $p < 0.05$, ** $p < 0.01$, **** $p < 0.00001$ vs the WT group; # $p < 0.01$ vs the TDP-43-Veh group).

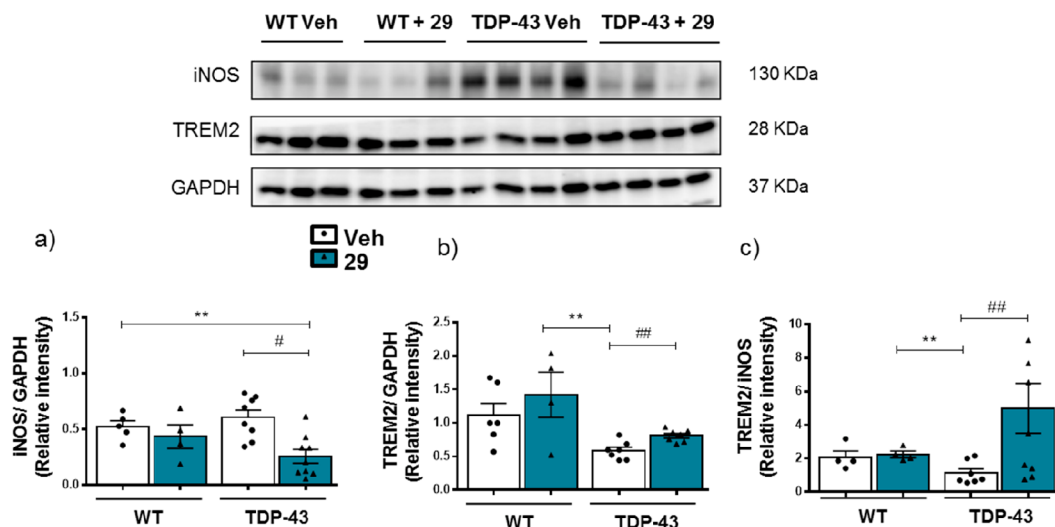


Figure 14. Immunomodulatory effect of compound 29 in the lumbar region of the spinal cord of wild-type and TDP-43 transgenic mice. Protein expression and desintometric data of (a) iNOS and (b) TREM2 and (c) the ratio TREM2/iNOS showing microglia switch from inflammatory M1-type to anti-inflammatory M2-type. GAPDH was used for endogenous normalization. Representative immunoblot are shown. Desintometric data represent the mean \pm SEM of different observations. Data were assessed by one-way ANOVA, followed by the Bonferroni test (** p < 0.01 vs WT group; $#p$ < 0.05, ## p < 0.01 vs the TDP-43-Veh group).

TTBK1 ligands were evaluated in a model of Tau-hyperphosphorylation induced by okadaic acid (OA).³⁵ In that assay, the compounds were able to rescue the SH-SY5Y cells from death induced by OA at two different compound concentrations of 1 and 5 μ M (Figure S6), confirming that our TTBK1 inhibitors in addition to TDP-43 also reduce the toxicity exerted by Tau-phosphorylation and expanding their therapeutic potential for different Tau-pathies.

2.5. Immunomodulatory Effect of TTBK1 Inhibition.

Chronic inflammation is another common feature observed in ALS, indicating the essential role of microglia in disease development and progression.³⁶ Thus, we decided to study the potential role of TTBK1 inhibition in microglia and its immunomodulatory effects. Therefore, we evaluated the effect of compound 29 on the expression of inducible nitric oxide synthase (iNOS) and the triggering receptor expressed on myeloid cells 2 (TREM2) in primary cultures of rat microglia after 24 h of exposure to the widely used pro-inflammatory stimulus lipopolysaccharide (LPS, 100 ng/mL). iNOS is widely considered a marker of M1 neurotoxic microglia, while TREM2 is considered a marker of M2 neuroprotective microglia. When cells were stimulated with LPS, we observed the expected iNOS induction, which was reduced by the treatment with compound 29, along with an increase in TREM2 expression (Figure 12), suggesting an immunomodulatory effect of the TTBK1 inhibitor 29. Compounds that induce the microglia switch from inflammatory M1-type to anti-inflammatory M2-type have been proposed to attenuate neuro-inflammation and bolster neuronal protection and recovery.³⁷

2.6. In Vivo TDP-43 Modulation by a TTBK1 Inhibitor.

Based in the promising results showed by the new TTBK1 inhibitors in cellular models, we explored the effects of compound 29 in the TDP-43 (A315T) transgenic mouse model, one of the first experimental models of ALS based on mutations in the TDP-43 protein.³⁸

First, we investigated the plasma pharmacokinetics and brain distribution of compound 29 in BALB/c wild-type mice following single intraperitoneal dose administration at 5 mg/kg

or oral administration at 10 mg/kg. Results are collected in Table 4 and show that compound 29 exhibits the greatest plasma concentration between 1 to 2 h, suggesting prolonged absorption and a high brain penetration in mice by the two routes of administration. Based on these results, we decided to use the intraperitoneal dose of 5 mg/kg in the efficacy study.

To this end, TDP-43 (A315T) transgenic mice and wild-type animals were treated daily with the TTBK1 inhibitor 29 or vehicle from the age of 65 days up to 95 days. The main goal of our study was to confirm the previously observed TDP-43 phosphorylation decrease and immunomodulatory effect of 29 together with the potential effect of these two relevant biological events in motor neuron preservation in the spinal cord.

We first analyzed whether chronic treatment with our TTBK1 inhibitor could prevent enhanced TDP-43 phosphorylation *in vivo*. Immunoblot analyses shown in Figure 13 revealed an increase in TDP-43 phosphorylation levels at the lumbar region in the spinal cord of transgenic mice compared to those in wild-type animals, which was statistically significantly reduced with compound 29 treatment (Figure 13a). No apparent effect on total levels of TDP-43 was appreciated between transgenic groups (Figure 13b).

We have already mentioned the pathogenic role of glial reactivity and related inflammatory processes in ALS neurodegeneration. To confirm the immunomodulatory effect of compound 29 *in vivo*, we examined iNOS and TREM2 protein expression in the spinal cord of TDP-43 (A315T) transgenic mice treated with 29 by Western Blot analysis. TDP-43 transgenic mice showed an increased in iNOS expression compared to wild type animals, which was significantly reduced in 29-treated animals (Figure 14a). This effect was accompanied by an increase in the anti-inflammatory microglial marker TREM2 (Figure 14b), confirming the microglia switch from the pro-inflammatory M1-type to the anti-inflammatory M2-type (Figure 14c) observed in the *in vitro* studies. Similar results were obtained by immunofluorescence analysis, where treatment with TTBK1 inhibitor 29 decreased

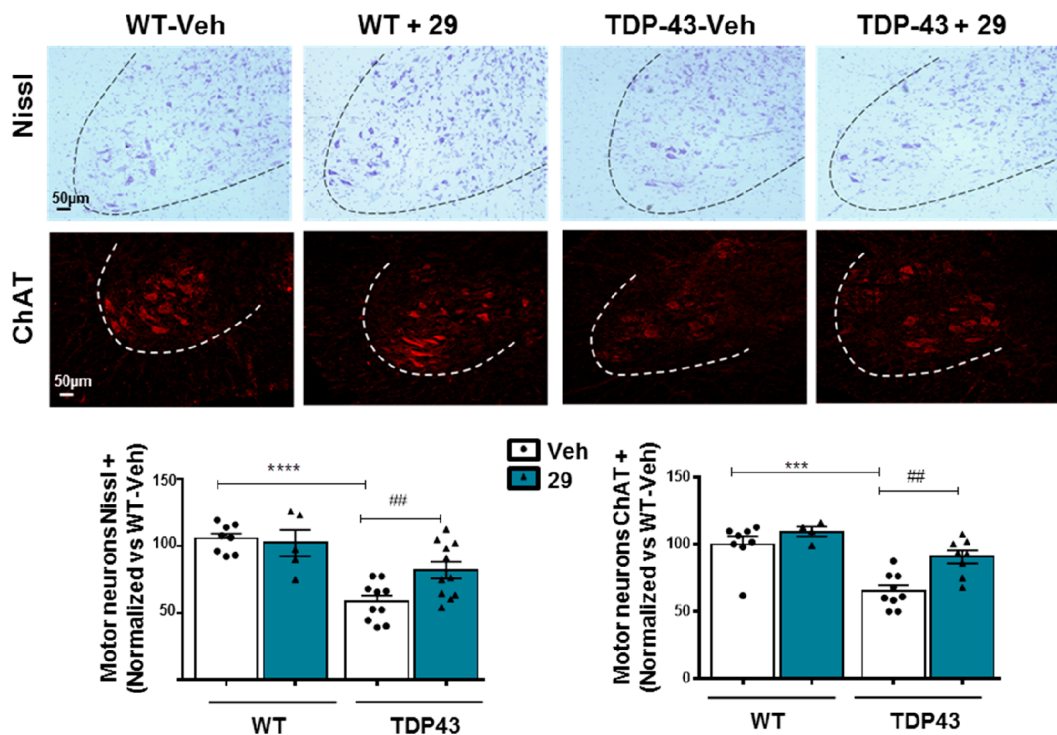


Figure 15. Representative images of Nissl-stained motor neurons and ChAT-immunostained sections in the anterior horn of the spinal cord of TDP-43 mice and wild-type treated with compound 29 or the vehicle. Quantification of the number of motor neurons Nissl+ and ChAT+ normalized vs WT-Veh is shown. Data were assessed by one-way ANOVA, followed by the Bonferroni test (**p < 0.01, ***p < 0.001, ****p < 0.0001 vs the WT-Veh group; ##p < 0.01 vs TDP-43-Veh).

the reactivity of both microglial (Iba-1) and astrocytes (GFAP) compared to the controls (Figure S7).

Finally, we investigated if the reduction of TDP-43 phosphorylation combined with the anti-inflammatory effect observed in the spinal cord of the transgenic mice treated with compound 29 contributed to an avoidance of motor neuron degeneration typical of this TDP-43 transgenic mice at advanced stages of disease progression. The reduction in the number of motor neurons observed in the ventral horn in transgenic animals as measured by two different markers, namely Nissl staining and choline acetyl transferase (ChAT) immunohistochemistry, was significantly prevented in those animals that received compound 29 as a treatment (Figure 15).

Taken together, these results demonstrate that TTBK1 inhibition is a potential, effective, and viable strategy to protect motor neuron degeneration in ALS and TDP-43 proteinopathies in murine models, and the pyrrolopyrimidine 29 may be a good drug candidate for further development.

2.7. TT BK1 Inhibitor Modulates TDP-43 Pathology in a Patient Cell-Based ALS Model. Finally, with the aim to help translate these promising results to the clinical setting, the modulatory effect of compounds 29 and 39 on the TDP-43 homeostasis was tested in a remarkable human cell-based model of the disease that was recently developed in our group. Cultures of immortalized lymphocytes from ALS patients recapitulate TDP-43 pathological features very well and represent a novel and effective platform to evaluate new drugs.³⁹ Lymphocytes were obtained from blood samples of patients or healthy individuals (Table 5) after written informed consent.

Thus, to confirm the privileged therapeutic profile of TT BK1 inhibitors in the modulation of TDP-43 proteinopathy, sporadic ALS-patient lymphoblasts were treated

Table 5. Demographic and Clinical Characteristics of Subjects Included in This Study^a

	control (n = 5)	ALS (n = 5)
gender (M/F)	(2/3)	(2/3)
age (±SD)	62 ± 7	65 ± 1
type of onset		
bulbar	NA	4
limb	NA	1

^aControl was individuals without signs of neurological degeneration; NA, not applicable. All patients were negative for SOD1, TARDBP, and C9orf72 mutations.

with both compounds for 24 h, resulting in reduced phosphorylation and cytosolic levels of TDP-43 with the simultaneous recovery of nuclear TDP-43 localization (Figure 16). These results highlight and demonstrate the importance of TT BK1 in the modulation of TDP-43 proteinopathy in a human cell-based model of sporadic ALS and reinforce the novelty of TT BK1 inhibition as an interesting approach for the pharmacological treatment of this devastating disease.

CONCLUSIONS

Overall, we have achieved the design, synthesis, and optimization of a new family of small molecules, resulting in rather potent and selective TT BK1 inhibitors based on a pyrrolopyrimidine scaffold. These compounds showed the ability to decrease TDP-43 phosphorylation both *in vitro* and in a TDP-43-transgenic mice model, demonstrating their relevance as lead structures for different TDP-43-pathies such as ALS. Moreover, in two different cellular models, including an ALS patient cell-based model, the developed TT BK1 inhibitors were able to recover the nuclear–cytosolic balance

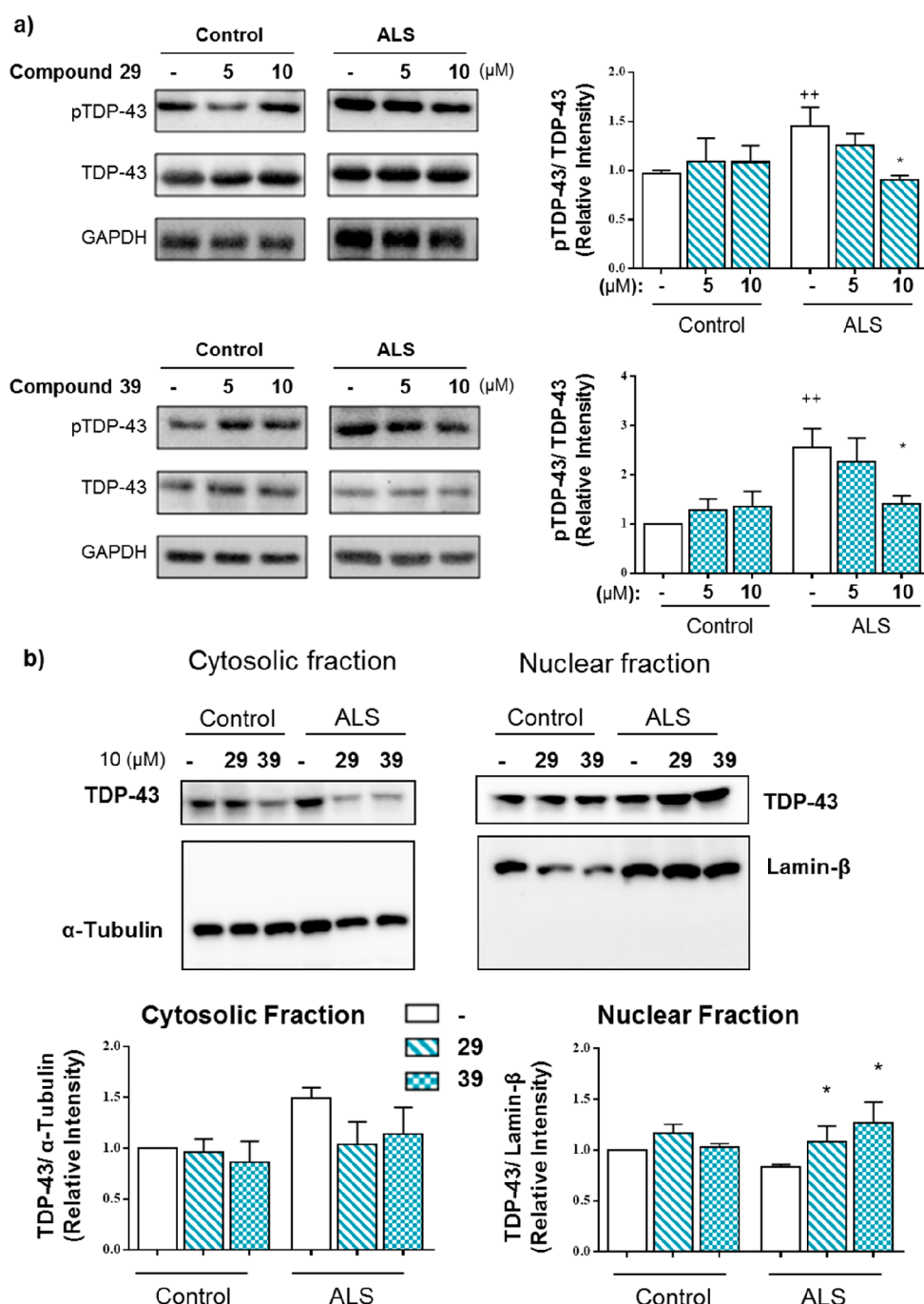


Figure 16. Effects of TTBK1 inhibitors on phosphorylation and subcellular localization of TDP-43 in ALS and control lymphoblasts. Twenty-four hours after the addition of compounds **29** and **39**, cells were harvested and processed for Western blotting analysis. (a) Representative immunoblots showing the effect of TTBK1 inhibitors decreasing TDP-43 phosphorylation. (b) Cytosolic and nuclear fractions analyzed by Western blotting. α -Tubulin and lamin B1 antibodies were used as loading and purity control for the cytosolic and nuclear fractions, respectively. Densitometric analyses represent the mean \pm SEM of different observations carried out in independent cell lines ($n = 5$) from each group (* $p < 0.05$ significantly different from ALS-untreated cells).

of TDP-43, which emphasizes the therapeutic potential of these compounds. Interestingly, experimentally calculated brain permeability predicted brain penetration for several compounds that was confirmed experimentally *in vivo* for compound **29**, showing a brain-to-plasma ratio of 3:1. In addition, crystal structures of ligand complexes for TTBK1 and TTBK2 can provide some new clues for specific TTBK1 modulation.

Altogether, we report a new family of TTBK1 inhibitors that for the first time modulate TDP-43 pathology in different models and can be considered new disease-modifying drugs for ALS and others TDP-43-pathies such as FTD, LATE, or Alexander's syndrome. Only future clinical trials will have the final confirmation of their therapeutic relevance.

■ EXPERIMENTAL SECTION

Chemistry. Reagents were obtained from the commercial sources and used without further purification. Purifications of crudes were performed with the indicated solvent as eluent by flash column chromatography carried out at medium pressure using either silica gel (E. Merck, grade 60, particle size 0.040–0.063 mm, 230–240 mesh ASTM) or the IsoleraOne flash purification system from Biotage. ¹H NMR and ¹³C NMR data were obtained from a Bruker AV300 or AV500 MHz spectrometer. Chemical shifts, δ , expressed in parts per million (ppm) were calculated taking the reference of the appropriated deuterated solvents. Signal multiplicities (bs = broad signal, s = singlet, d = doublet, dd = doublet of doublets, ddd = doublet of doublet of doublets, t = triplet, td = triplet of doublets, q = quartet, and m = multiplet) and coupling constants (J , Hz) are indicated for each molecule. Acquired spectroscopic data were analyzed with MestreNova 10.2 software. The microwave-assisted synthesis was carried out using a Biotage Initiator eight single-mode cavity instrument from Biotage. Experiments were performed with the temperature control mode in sealed microwave process vials. The temperature was measured with an IR sensor on the outside of the reaction vessel. Stirring was provided by an *in situ* magnetic stirrer. High-performance liquid chromatography (HPLC) analyses were performed in a Thermo Finnigan Surveyor UV-vis Plus detector coupled with FinniganTM LXQ TM system. The column used for the analysis was a SunFire C18 (3.5 μ m, 4.6 \times 50 mm), and UV-vis spectra of the samples were acquired. Melting points were determined in a Büchi Melting Point M-560 apparatus. High-resolution mass spectrometry (HRMS) was done in an Agilent 6500 spectrometer using positive electrospray techniques (ESI). Values are expressed in mass units (*m/z*). Elemental analyses were performed by the analytical department at CAI-UCM using the analyzer LECO CHNS-932, and the results obtained were within $\pm 0.4\%$ of the theoretical values. All the final compounds have purities $\geq 95\%$ as tested by HPLC.

General Procedure for the Synthesis of Derivatives 1–55. (a) First, 1 equiv of 6-chloro-7-deazapurine, 6-chloropurine, or 6-chlorothienopirimidine; 1 equiv of the corresponding aniline; and 0.1 equiv of indium trichloride were dissolved in 2 mL of acetonitrile. The crude was stirred under microwave irradiation at 100 °C until the completion of the reaction. (b) First, 1 equiv of 6-chloro-7-deazapurine, 6-chloropurine, or 6-chlorothienopirimidine and 1 equiv of the corresponding aniline were dissolved in 2 mL of tetrahydrofuran. The crude was stirred under microwave irradiation at 100 °C until the completion of the reaction.

The corresponding crude was extracted using 20 mL of EtOAc and washed with NaHCO₃ and brine. The organic layer was dried over MgSO₄ and evaporated under high vacuum. The corresponding crude was purified using flash chromatography and CH₂Cl₂/MeOH 40:1 as the eluent.

3-((9*H*-Purine-6-il)amino)phenol (1). Yield 29%. Mp 339–340 °C. ¹H NMR (500 MHz, DMSO-*d*₆): δ (ppm) 13.16 (s, 1H), 9.61 (s, 1H), 9.31 (s, 1H), 8.36 (s, 1H), 8.26 (s, 1H), 7.55 (s, 1H), 7.32 (m, 1H), 7.08 (m, 1H), 6.42 (m, 1H). ¹³C NMR (125 MHz, DMSO-*d*₆): δ (ppm) 158.2, 152.8, 150.9, 141.1, 140.0, 128.1, 124.1, 120.0, 112.8, 110.0, 108.3. ESI: calcd for C₁₁H₉N₅O [M + H]⁺ 228.0880. Found: 228.0877

(N-(4-Phenoxy)-9*H*-purin-6-amino)phenol (2). Yield 20%. Mp 336–338 °C. ¹H NMR (300 MHz, DMSO-*d*₆): δ (ppm) 13.06 (s, 1H), 9.47 (s, 1H), 9.14 (s, 1H), 8.26 (s, 1H), 8.20 (s, 1H), 7.64 (d, J = 8.7 Hz, 2H), 6.72 (d, J = 8.8 Hz, 2H). ¹³C NMR (75 MHz, DMSO-*d*₆): δ (ppm) 153.1, 152.1, 151.9, 150.1, 139.3, 131.2, 122.8, 121.1, 119.1, 114.8. ESI: calcd for C₁₁H₉N₅O [M + H]⁺ 228.0880. Found: 228.0879

(N-(4-Morpholinophenyl)-9*H*-purin-6-amino)phenol (3). Yield 70%. Mp 269–270 °C. ¹H NMR (300 MHz, DMSO-*d*₆): δ (ppm) 13.05 (s, 1H), 9.58 (s, 1H), 8.31 (s, 1H), 8.24 (s, 1H), 7.75 (d, J = 9.0 Hz, 2H), 6.92 (d, J = 9.1 Hz, 2H), 3.74 (t, J = 4.2 Hz, 4H), 3.05 (t, J = 4.7 Hz, 4H). ¹³C NMR (75 MHz, DMSO-*d*₆): δ (ppm) 151.9, 151.6,

150.9, 146.9, 139.9, 132.0, 121.9, 118.4, 115.4, 66.2, 49.1. ESI: calcd for C₁₅H₁₆N₆O [M + H]⁺ 297.1458. Found: 297.1457

(N-(4-Chlorophenyl)-9*H*-purin-6-amino) (4). Yield 75%. Mp 329–330 °C. ¹H NMR (500 MHz, DMSO-*d*₆): δ (ppm) 13.21 (s, 1H), 9.95 (s, 1H), 8.40 (s, 1H), 8.30 (s, 1H), 8.03 (d, J = 8.9 Hz, 2H), 7.37 (d, J = 8.9 Hz, 2H). ¹³C NMR (126 MHz, DMSO-*d*₆): δ (ppm) 151.7, 151.6, 150.6, 140.2, 138.9, 128.2, 125.8, 121.8, 119.5. ESI: calcd for C₁₁H₈ClN₅ [M + H]⁺ 246.0541. Found: 246.0542

N-4-Chlorophenylthieno[2,3-*d*]pyrimidin-4-amine (5). Yield 50%. Mp 179–180 °C. ¹H NMR (300 MHz, DMSO-*d*₆): δ (ppm) 9.75 (s, 1H), 8.52 (s, 1H), 7.95–7.84 (m, 3H), 7.75 (d, J = 6.0 Hz, 1H), 7.43 (d, J = 8.9 Hz, 2H). ¹³C NMR (75 MHz, DMSO-*d*₆): δ (ppm) 166.6, 154.6, 153.0, 138.3, 128.5, 126.8, 124.2, 122.8, 119.4, 117.0. Anal. Calcd for C₁₂H₈ClN₃S: C, 49.92; H, 3.84; N, 14.55; S 11.10. Found C, 50.22; H, 3.13; N, 14.09; S 10.76.

N-Phenylthieno[2,3-*d*]pyrimidin-4-amine (6). Yield 70%. Mp 175–176 °C. ¹H NMR (300 MHz, DMSO-*d*₆): δ (ppm) 9.65 (s, 1H), 8.49 (s, 1H), 7.89 (d, J = 6.0 Hz, 1H), 7.86–7.81 (m, 2H), 7.73 (d, J = 5.9 Hz, 1H), 7.46–7.31 (m, 2H), 7.16–7.04 (m, 1H). ¹³C NMR (75 MHz, DMSO-*d*₆): δ (ppm) 166.5, 154.8, 153.2, 139.2, 128.5, 123.8, 123.3, 121.5, 119.5, 116.9. Anal. Calcd for C₁₂H₉N₃S: C, 63.41; H, 3.99; N, 18.49; S 14.11. Found: C, 63.36; H, 4.16; N, 18.46; S 14.07.

N-(3-Phenol)-7*H*-pirrolo[2,3-*d*]pyrimidin-4-amine (7). Yield 87%. Mp 253–255 °C. ¹H NMR (300 MHz, DMSO-*d*₆): δ (ppm) 11.75 (s, 1H), 9.34 (s, 1H), 9.17 (s, 1H), 8.28 (s, 1H), 7.50 (s, 1H), 7.26 (dd, J = 2.0, 7.9 Hz, 1H), 7.22 (dd, J = 3.5, 1.7 Hz, 1H), 7.10 (t, J = 8.0 Hz, 1H), 6.80 (d, J = 3.5 Hz, 1H), 6.43 (dd, J = 8.0, 2.3 Hz, 1H). ¹³C NMR (75 MHz, DMSO-*d*₆): δ (ppm) 157.8, 153.9, 151.2, 151.0, 141.8, 129.4, 122.4, 111.5, 109.6, 107.7, 104.1, 99.2. ESI: calcd for C₁₂H₁₀N₄O [M + H]⁺ 227.0927. Found: 227.0929.

N-(4-Phenol)-7*H*-pyrrolo[2,3-*d*]pyrimidin-4-amine (8). Yield 38%. Mp 274–276 °C. ¹H NMR (300 MHz, DMSO-*d*₆): δ (ppm) 11.65 (s, 1H), 9.17 (s, 1H), 9.05 (s, 1H), 8.18 (s, 1H), 7.56 (d, J = 8.8 Hz, 2H), 7.17 (dd, J = 3.5, 2.3 Hz, 1H), 6.77 (d, J = 8.8 Hz, 2H), 6.63 (dd, J = 3.5, 2.1 Hz, 1H). ¹³C NMR (75 MHz, DMSO-*d*₆): δ (ppm) 154.0, 153.0, 150.9, 150.6, 131.6, 123.0, 121.4, 114.9, 103.0, 98.8. ESI: calcd for C₁₂H₁₀N₄O [M + H]⁺ 227.0927. Found: 227.0925.

N-(4-Morpholinophenyl)-7*H*-pyrrolo[2,3-*d*]pyrimidin-4-amine (9). Yield 24%. Mp 254–255 °C. ¹H NMR (300 MHz, DMSO-*d*₆): δ (ppm) 11.65 (s, 1H), 9.10 (s, 1H), 8.20 (s, 1H), 7.67 (d, J = 7.2 Hz, 2H), 7.17 (dd, J = 3.5, 2.3 Hz, 1H), 6.94 (d, J = 6.9 Hz, 2H), 6.67 (dd, J = 3.5, 1.8 Hz, 1H), 3.74 (t, J = 9.4, 4.9 Hz, 4H), 3.06 (t, J = 9.2, 4.7 Hz, 4H). ¹³C NMR (75 MHz, DMSO-*d*₆): δ (ppm) 153.8, 150.9, 150.7, 146.7, 132.5, 122.0, 121.6, 115.4, 103.2, 98.8, 66.1, 49.1. ESI: calcd for C₁₆H₁₇N₅O [M + H]⁺ 296.1506. Found: 296.1496.

N-(4-Chlorophenyl)-7*H*-pyrrolo[2,3-*d*]pyrimidin-4-amine (10). Yield 92%. Mp 259–260 °C. ¹H NMR (300 MHz, DMSO-*d*₆): δ (ppm) 11.82 (s, 1H), 9.43 (s, 1H), 8.30 (s, 1H), 7.97 (dt, J = 8.9, 2.0 Hz, 2H), 7.38 (dt, 2H), 7.26 (dd, J = 3.5, 2.3 Hz, 1H), 6.80 (dd, J = 3.5, 1.9 Hz, 1H). ¹³C NMR (75 MHz, DMSO-*d*₆): δ (ppm) 153.2, 150.9, 150.6, 139.5, 128.3, 125.3, 122.4, 121.4, 103.8, 98.7. Anal. Calcd for C₁₂H₉ClN₄: C, 58.91; H, 3.71; N, 22.90. Found: C, 58.66; H, 3.78; N, 22.83.

N-(4-Chlorobenzyl)-7*H*-pyrrolo[2,3-*d*]pyrimidin-4-amine (11). Yield 55%. Mp 208–209 °C. ¹H NMR (300 MHz, DMSO-*d*₆): δ (ppm) 11.53 (s, 1H), 8.08 (s, 1H), 7.97 (t, J = 6.1 Hz, 1H), 7.36 (s, 4H), 7.08 (dd, J = 3.4, 2.3 Hz, 1H), 6.56 (dd, J = 3.4, 1.9 Hz, 1H), 4.69 (d, J = 6.1 Hz, 2H). ¹³C NMR (75 MHz, DMSO-*d*₆): δ (ppm) 156.2, 151.7, 150.5, 139.9, 131.4, 129.4, 129.4, 128.5, 121.4, 102.9, 98.9, 42.8. Anal. Calcd for C₁₃H₁₁ClN₄: C, 60.35; H, 4.29; N, 21.66. Found: C, 60.35; H, 4.24; N, 21.47.

N-(4-Chloroethylphenyl)-7*H*-pyrrolo[2,3-*d*]pyrimidin-4-amine (12). Yield 25%. Mp 207–208 °C. ¹H NMR (300 MHz, DMSO-*d*₆): δ (ppm) 11.48 (s, 1H), 8.12 (s, 1H), 7.47 (t, J = 5.7 Hz, 1H), 7.43–7.18 (m, 4H), 7.05 (dd, J = 3.4, 2.2 Hz, 1H), 6.51 (dd, J = 3.4, 1.7 Hz, 1H), 3.67 (q, J = 7.2, 5.8 Hz, 2H), 2.91 (t, J = 7.3 Hz, 2H). ¹³C NMR (75 MHz, DMSO-*d*₆): δ (ppm) 156.0, 151.5, 150.1, 138.9, 130.7, 130.6, 128.2, 120.8, 102.6, 98.5, 41.4, 34.6. ESI: calcd for C₁₄H₁₄ClN₄ [M + H]⁺ 273.0902. Found: 273.0895.

4-((7H-Pyrrolo[2,3-d]pyrimidin-4-yl)amino)methylphenol (13). Yield 14%. Mp 206–207 °C. ^1H NMR (300 MHz, DMSO- d_6): δ (ppm) 11.49 (s, 1H), 9.27 (s, 1H), 8.10 (s, 1H), 7.81 (t, 1H), 7.15 (d, J = 8.3 Hz, 2H), 7.05 (t, J = 2.7 Hz, 1H), 6.69 (d, J = 8.5 Hz, 2H), 6.57 (dd, J = 3.5, 1.7 Hz, 1H), 4.58 (d, J = 5.8 Hz, 2H). ^{13}C NMR (75 MHz, DMSO- d_6): δ (ppm) 156.2, 156.0, 151.5, 150.2, 130.5, 128.7, 120.8, 115.0, 102.5, 98.7, 42.7. ESI: calcd for $\text{C}_{13}\text{H}_{12}\text{N}_4\text{O}$ [M + H]⁺ 241.1084. Found: 241.1079

4-(2-((7H-Pyrrolo[2,3-d]pyrimidin-4-yl)amino)ethyl)phenol (14). Yield 23%. Mp 246–247 °C. ^1H NMR (300 MHz, DMSO- d_6): δ (ppm) 11.47 (s, 1H), 9.18 (s, 1H), 8.11 (s, 1H), 7.45 (t, J = 5.7 Hz, 1H), 7.09–7.01 (m, 3H), 6.68 (d, J = 8.4 Hz, 2H), 6.52 (dd, J = 3.4, 1.7 Hz, 1H), 3.68–3.48 (m, 2H), 2.79 (t, J = 7.6 Hz, 2H). ^{13}C NMR (75 MHz, DMSO- d_6): δ (ppm) 156.0, 155.6, 151.5, 150.1, 129.8, 129.5, 120.7, 115.1, 102.5, 98.6, 42.1, 34.6. ESI: calcd for $\text{C}_{14}\text{H}_{14}\text{N}_4\text{O}$ [M + H]⁺ 255.1240. Found: 255.1239

N-(3-Chlorophenyl)-7H-pyrrolo[2,3-d]pyrimidin-4-amine (15). Yield 49%. Mp 234–235 °C (lit⁴⁰ 227–228 °C). ^1H NMR (500 MHz, DMSO- d_6): δ (ppm) 12.81 (s, 1H), 11.42 (s, 1H), 8.45 (s, 1H), 7.90 (s, 1H), 7.66 (m, 1H), 7.50 (m, 1H), 7.45 (m, 1H), 7.34 (m, 1H), 7.26 (m, 1H). ^{13}C NMR (125 MHz, DMSO- d_6): δ (ppm) 151.4, 146.1, 144.7, 138.7, 133.7, 131.2, 125.9, 125.0, 123.7, 122.6, 102.37, 102.3. ESI: calcd for $\text{C}_{12}\text{H}_9\text{ClN}_4$ [M + H]⁺ 245.0589. Found: 245.0587

N-(2-Chlorophenyl)-7H-pyrrolo[2,3-d]pyrimidin-4-amine (16). Yield 69%. Mp 220–221 °C. ^1H NMR (300 MHz, DMSO- d_6): δ (ppm) 11.73 (s, 1H), 9.07 (s, 1H), 8.13 (s, 1H), 7.69 (dd, J = 8.0, 1.6 Hz, 1H), 7.54 (dd, J = 8.0, 1.6 Hz, 1H), 7.37 (dt, J = 7.7, 1.6 Hz, 1H), 7.24 (dt, J = 7.6, 1.7 Hz, 1H), 7.14 (dd, J = 3.5, 2.3 Hz, 1H), 6.51 (dd, J = 3.5, 1.8 Hz, 1H). ^{13}C NMR (75 MHz, DMSO- d_6): δ (ppm) 154.3, 151.1, 150.9, 136.4, 129.5, 129.4, 128.5, 127.3, 126.4, 122.2, 103.1, 98.7. Anal. Calcd for $\text{C}_{12}\text{H}_9\text{ClN}_4$: C, 58.91; H, 3.71; N, 22.90. Found: C, 58.77; H, 3.79; N, 22.90.

N-(2-Phenoxy)-7H-pyrrolo[2,3-d]pyrimidin-4-amine (17). Yield 20%. Mp 233–235 °C. ^1H NMR (300 MHz, DMSO- d_6): δ (ppm) 11.82 (s, 1H), 10.61 (s, 1H), 8.91 (s, 1H), 8.22 (s, 1H), 7.56 (dd, J = 7.9, 1.6 Hz, 1H), 7.22 (dd, J = 3.5, 2.3 Hz, 1H), 7.02 (ddd, J = 8.0, 7.1, 1.6 Hz, 1H), 6.92 (dd, J = 8.0, 1.6 Hz, 1H), 6.84 (ddd, J = 7.9, 7.2, 1.6 Hz, 1H), 6.70 (dd, J = 3.5, 1.8 Hz, 1H). ^{13}C NMR (75 MHz, DMSO- d_6): δ (ppm) 153.8, 150.6, 150.2, 149.6, 127.8, 125.0, 124.3, 122.2, 119.1, 117.4, 103.2, 99.1. ESI: calcd for $\text{C}_{12}\text{H}_{10}\text{N}_4\text{O}$ [M + H]⁺ 227.0927. Found: 227.0926

N-(5,6,7,8-Tetrahydronaphthalen-1-yl)-7H-pyrrolo[2,3-d]pyrimidin-4-amine (18). Yield 23%. Mp 239–240 °C. ^1H NMR (300 MHz, DMSO- d_6): δ (ppm) 11.58 (s, 1H), 8.74 (s, 1H), 8.06 (s, 1H), 7.20–7.05 (m, 3H), 6.99 (dd, J = 7.3, 1.7 Hz, 1H), 6.22 (dd, J = 3.2, 1.5 Hz, 1H), 2.78 (t, J = 5.3 Hz, 2H), 2.61 (t, J = 5.3 Hz, 2H), 1.68 (t, J = 3.4 Hz, 4H). ^{13}C NMR (75 MHz, DMSO- d_6): δ (ppm) 155.7, 151.6, 151.5, 138.0, 137.9, 134.0, 127.0, 125.6, 125.2, 121.9, 103.0, 99.4, 29.7, 25.0, 22.9 (C-18–19). Anal. Calcd for $\text{C}_{16}\text{H}_{16}\text{N}_4$: C, 72.70; H, 6.10; N, 21.70. Found: C, 72.50; H, 6.05; N, 21.22.

N-(Benzod[1,3]dioxol-5-yl)-7H-pyrrolo[2,3-d]pyrimidin-4-amine (19). Yield 15%. Mp 282–283 °C. ^1H NMR (300 MHz, DMSO- d_6): δ (ppm) 11.69 (s, 1H), 9.17 (s, 1H), 8.22 (s, 1H), 7.58 (d, J = 2.1 Hz, 1H), 7.23–7.15 (m, 2H), 6.89 (d, J = 8.4 Hz, 1H), 6.70 (dd, J = 3.5, 1.9 Hz, 1H), 6.00 (s, 2H). ^{13}C NMR (75 MHz, DMSO- d_6): δ (ppm) 153.6, 150.77, 150.72, 146.9, 142.3, 134.7, 121.9, 113.3, 107.8, 103.3, 103.0, 100.8, 98.7. ESI: calcd for $\text{C}_{13}\text{H}_{10}\text{N}_4\text{O}_2$ [M + H]⁺ 255.0877. Found: 255.0877.

1-(4-((7H-Pyrrolo[2,3-d]pyrimidin-4-yl)amino)phenyl)ethan-1-one (20). Yield 25%. Mp 279–280 °C. ^1H NMR (300 MHz, DMSO- d_6): δ (ppm) 11.87 (s, 1H), 9.67 (s, 1H), 8.38 (s, 1H), 8.11 (d, J = 8.8 Hz, 2H), 7.96 (d, J = 8.8 Hz, 2H), 7.31 (dd, J = 3.5, 2.3 Hz, 1H), 6.87 (dd, J = 3.5, 1.9 Hz, 1H). ^{13}C NMR (75 MHz, DMSO- d_6): δ (ppm) 196.6, 153.2, 151.5, 150.9, 145.5, 130.5, 129.7, 123.3, 119.0, 104.7, 99.1, 26.7. Anal. Calcd for $\text{C}_{14}\text{H}_{12}\text{N}_4\text{O}$: C, 65.07; H, 5.80; N, 23.71. Found: C, 64.88; H, 5.68; N, 23.20

N-(3-Morpholinophenyl)-7H-pyrrolo[2,3-d]pyrimidin-4-amine (21). Yield 58%. Mp 258–259 °C. ^1H NMR (300 MHz, DMSO- d_6): δ (ppm) 11.65 (s, 1H), 9.10 (s, 1H), 8.20 (s, 1H), 7.67 (dd, J = 7.2, 2.2

Hz, 2H), 7.17 (dd, J = 3.5, 2.3 Hz, 1H), 6.94 (dd, J = 6.9, 2.1 Hz, 2H), 6.67 (dd, J = 3.5, 1.8 Hz, 1H), 3.74 (t, J = 9.4, 4.9 Hz, 4H), 3.06 (t, J = 9.2, 4.7 Hz, 4H). ^{13}C NMR (75 MHz, DMSO- d_6): δ (ppm) 153.6, 151.4, 150.8, 150.8, 141.1, 128.8, 122.0, 111.7, 109.4, 107.2, 103.6, 98.7, 66.1, 48.7. Anal. Calcd for $\text{C}_{16}\text{H}_{17}\text{N}_5\text{O}$: C, 65.07; H, 5.80; N, 23.71. Found: C, 64.88; H, 5.68; N, 23.20.

N-Phenyl-7H-pyrrolo[2,3-d]pyrimidin-4-amine (22). Yield 64%. Mp 239–240 °C. ^1H NMR (300 MHz, DMSO- d_6): δ (ppm) 11.75 (s, 1H), 9.29 (s, 1H), 8.28 (s, 1H), 7.89 (dd, J = 7.5, 1.0 Hz, 2H), 7.33 (td, J = 8.7, 2.1 Hz, 2H), 7.23 (dd, J = 3.5, 2.3 Hz, 1H), 7.01 (tt, J = 7.2, 2.4, 1.1 Hz, 1H), 6.79 (dd, J = 3.5, 1.8 Hz, 1H). ^{13}C NMR (75 MHz, DMSO- d_6): δ (ppm) 153.5, 150.8, 150.7, 140.4, 128.4, 122.1, 122.0, 120.2, 103.6, 98.8. ESI: calcd for $\text{C}_{12}\text{H}_{10}\text{N}_4$ [M + H]⁺ 211.0978. Found: 211.0979.

N-(4-Methoxyphenyl)-7H-pyrrolo[2,3-d]pyrimidin-4-amine (23). Yield 74%, Mp 229–230 °C. ^1H NMR (300 MHz, DMSO- d_6): δ (ppm) 11.66 (s, 1H), 9.14 (s, 1H), 8.20 (s, 1H), 7.71 (d, J = 9.0 Hz, 2H), 7.18 (dd, J = 3.5, 2.3 Hz, 1H), 6.92 (d, J = 9.0 Hz, 2H), 6.67 (dd, J = 3.5, 1.9 Hz, 1H), 3.75 (s, 3H). ^{13}C NMR (75 MHz, DMSO- d_6): δ (ppm) 156.2, 156.0, 151.5, 150.2, 130.5, 128.7, 120.8, 115.0, 102.5, 98.7, 42.7. Anal. Calcd for $\text{C}_{13}\text{H}_{12}\text{N}_4\text{O}$: C, 64.99; H, 5.03; N, 23.32. Found: C, 64.59; H, 5.03; N, 23.03.

N-(4-(Trifluoromethoxy)phenyl)-7H-pyrrolo[2,3-d]pyrimidine-4-amine (24). Yield 92%, Mp 202–203 °C. ^1H NMR (300 MHz, DMSO- d_6): δ (ppm) 11.81 (s, 1H), 9.47 (s, 1H), 8.29 (s, 1H), 8.02 (d, J = 9.1 Hz, 2H), 7.34 (dd, J = 9.2, 1.0 Hz, 2H), 7.26 (dd, J = 3.5, 2.3 Hz, 1H), 6.80 (dd, J = 3.5, 1.9 Hz, 1H). ^{13}C NMR (75 MHz, DMSO- d_6): δ (ppm) 153.2, 151.0, 150.6, 142.6 (d, J = 1.9 Hz), 139.7, 122.5, 121.4, 121.2, 120.2 (d, J = 255.3 Hz), 103.8, 98.7. Anal. Calcd for $\text{C}_{13}\text{H}_9\text{F}_3\text{N}_4\text{O}$: C, 53.07; H, 3.08; N, 19.04. Found: C, 52.81; H, 3.16; N, 18.99.

N-(4-Isopropoxypyhenyl)-7H-pyrrolo[2,3-d]pyrimidin-4-amine (25). Yield 66%. Mp 218–219 °C. ^1H NMR (300 MHz, DMSO- d_6): δ (ppm) 11.66 (s, 1H), 9.13 (s, 1H), 8.20 (s, 1H), 7.69 (d, J = 9.0 Hz, 2H), 7.17 (dd, J = 3.5, 2.3 Hz, 1H), 6.89 (d, J = 9.0 Hz, 2H), 6.68 (dd, J = 3.5, 1.8 Hz, 1H), 4.54 (hept, J = 6.0, 1H), 1.26 (d, J = 6.0, 6H). ^{13}C NMR (75 MHz, DMSO- d_6): δ (ppm) 153.8, 150.9, 150.7, 133.2, 122.4, 121.7, 115.7, 103.2, 98.8, 69.4, 21.9 ESI: calcd for $\text{C}_{15}\text{H}_{16}\text{N}_4\text{O}$ [M + H]⁺ 269.1397. Found: 269.1393.

N-(4-Etoxyphenyl)-7H-pyrrolo[2,3-d]pyrimidin-4-amine (26). Yield 20%. Mp 241–242 °C. ^1H NMR (300 MHz, DMSO- d_6): δ (ppm) 11.66 (s, 1H), 9.13 (s, 1H), 8.20 (s, 1H), 7.70 (d, J = 9.1 Hz, 2H), 7.17 (dd, J = 3.4, 2.3 Hz, 1H), 6.91 (d, J = 9.1 Hz, 2H), 6.67 (dd, J = 3.5, 1.9 Hz, 1H), 4.00 (q, J = 7.0, 2H), 1.33 (d, J = 7.0, 3H). ^{13}C NMR (75 MHz, DMSO- d_6): δ (ppm) 154.0, 153.8, 150.9, 150.7, 133.2, 122.4, 121.7, 114.2, 103.2, 98.8, 63.1, 14.8. ESI: calcd for $\text{C}_{14}\text{H}_{14}\text{N}_4\text{O}$ [M + H]⁺ 255.1240. Found: 255.1236.

N-(4-Phenoxyphenyl)-7H-pyrrolo[2,3-d]pyrimidin-4-amine (27). Yield 53%. Mp 250–251 °C. ^1H NMR (300 MHz, DMSO- d_6): δ (ppm) 11.75 (s, 1H), 9.34 (s, 1H), 8.26 (s, 1H), 7.89 (d, J = 9.0 Hz, 2H), 7.37 (dd, J = 8.6, 7.3 Hz, 2H), 7.23 (dd, J = 3.5, 2.3 Hz, 1H), 7.13–6.96 (m, 5H), 6.77 (dd, J = 3.5, 1.9 Hz, 1H). ^{13}C NMR (75 MHz, DMSO- d_6): δ (ppm) 157.6, 153.5, 150.8, 150.75, 150.7, 136.3, 129.9, 122.7, 122.1, 122.0, 119.4, 117.6, 103.5, 98.7. Anal. Calcd for $\text{C}_{18}\text{H}_{14}\text{N}_4\text{O}$: C, 71.51; H, 7.67; N, 18.53. Found: C, 71.04; H, 4.70; N, 18.38.

N-Cyclohexyl-7H-pyrrolo[2,3-d]pyrimidin-4-amine (28). Yield 26%. Mp 146–147 °C. ^1H NMR (300 MHz, DMSO- d_6): δ (ppm) 11.41 (s, 1H), 8.06 (s, 1H), 7.09 (d, J = 7.9 Hz, 1H), 7.03 (dd, J = 3.4, 2.2 Hz, 1H), 6.57 (dd, J = 3.4, 1.8 Hz, 1H), 4.12–3.95 (m, 1H), 2.00–1.87 (m, 2H), 1.82–1.74 (m, 2H), 1.74–1.56 (m, 2H), 1.44–1.22 (m, 4H). ^{13}C NMR (75 MHz, DMSO- d_6): δ (ppm) 155.3, 151.4, 150.2, 120.4, 102.3, 98.7, 48.5, 32.8, 25.5, 25.0. ESI: calcd for $\text{C}_{12}\text{H}_{16}\text{N}_4$ [M + H]⁺ 217.1448. Found: 217.1439.

N-(4-(4-Chlorophenoxy)phenyl)-7H-pyrrolo[2,3-d]pyrimidin-4-amine (29). Yield 62%. Mp 250–251 °C. ^1H NMR (300 MHz, DMSO- d_6): δ (ppm) 11.77 (s, 1H), 9.36 (s, 1H), 8.26 (s, 1H), 7.92 (d, J = 9.0 Hz, 2H), 7.41 (d, J = 9.0 Hz, 2H), 7.24 (dd, J = 3.4, 2.3 Hz, 1H), 7.06 (d, J = 9.0 Hz, 2H), 7.00 (d, J = 9.0 Hz, 2H), 6.77 (dd, J = 3.5, 1.9 Hz, 1H). ^{13}C NMR (75 MHz, DMSO- d_6): δ (ppm) 156.7,

153.4, 150.8, 150.7, 150.2, 136.8, 129.7, 126.4, 122.1, 121.9, 119.7, 119.2, 103.5, 98.7. Anal. Calcd for $C_{18}H_{13}ClN_4O$: C, 64.20; H, 3.89; N, 16.64. Found: C, 65.15; H, 3.96; N, 16.69.

N-(4-(4-Fluorophenoxy)phenyl)-7H-pyrrolo[2,3-d]pyrimidin-4-amine (30). Yield 40%. Mp 227–228 °C. 1H NMR (300 MHz, DMSO- d_6): δ (ppm) 11.75 (s, 1H), 9.33 (s, 1H), 8.25 (s, 1H), 7.88 (d, J = 9.0 Hz, 2H), 7.26–7.15 (m, 3H), 7.08–6.95 (m, 4H), 6.76 (dd, J = 3.5, 1.9 Hz, 1H). ^{13}C NMR (75 MHz, DMSO- d_6): δ (ppm) 159.4 (d, J = 238.1 Hz), 153.6 (d, J = 2.3 Hz), 153.5, 151.3, 150.8, 136.3, 122.1, 122.0, 119.6 (d, J = 8.4 Hz), 119.0, 116.4 (d, J = 23.3 Hz), 103.5, 98.7. Anal. Calcd for $C_{18}H_{13}FN_4O$: C, 67.49; H, 4.09; N, 17.49. Found: C, 67.09; H, 4.09; N, 17.38.

N-(4-(4-Cianophenoxy)phenyl)-7H-pyrrolo[2,3-d]pyrimidin-4-amine (31). Yield 6%. Mp 259–260 °C. 1H NMR (300 MHz, DMSO- d_6): δ (ppm) 11.77 (s, 1H), 9.41 (s, 1H), 8.28 (s, 1H), 7.99 (d, J = 9.0 Hz, 2H), 7.83 (d, J = 8.9 Hz, 2H), 7.25 (dd, J = 3.5, 2.3 Hz, 1H), 7.15 (d, J = 9.0 Hz, 2H), 7.09 (d, J = 8.9 Hz, 2H), 6.79 (dd, J = 3.5, 1.8 Hz, 1H). ^{13}C NMR (75 MHz, DMSO- d_6): δ (ppm) 161.9, 153.3, 150.8, 150.7, 148.4, 137.8, 134.6, 122.2, 121.8, 120.7, 118.8, 117.3, 104.5, 103.6, 98.7. Anal. Calcd for $C_{19}H_{13}N_5O$: C, 69.71; H, 4.00; N, 21.39. Found: C, 69.33; H, 4.15; N, 21.01.

N-(4-(4-Methoxyphenoxy)phenyl)-7H-pyrrolo[2,3-d]pyrimidin-4-amine (32). Yield 63%. Mp 202–203 °C. 1H NMR (300 MHz, DMSO- d_6): δ (ppm) 11.74 (s, 1H), 9.30 (s, 1H), 8.25 (s, 1H), 7.84 (d, J = 9.0 Hz, 2H), 7.23 (dd, J = 3.5, 2.3 Hz, 1H), 7.04–6.94 (m, 6H), 6.76 (dd, J = 3.1, 1.9 Hz, 1H), 3.76 (s, 3H). ^{13}C NMR (75 MHz, DMSO- d_6): δ (ppm) 155.2, 153.5, 152.4, 150.8, 150.7, 150.4, 135.5, 122.0, 121.9, 119.8, 118.0, 115.0, 103.4, 98.7, 55.4. Anal. Calcd for $C_{19}H_{16}N_4O_2$: C, 68.66; H, 4.85; N, 16.86. Found: C, 67.97; H, 4.91; N, 16.64.

N-(4-(4-Trifluoromethylphenoxy)phenyl)-7H-pyrrolo[2,3-d]pyrimidin-4-amine (33). Yield 74%. Mp 233–234 °C. 1H NMR (300 MHz, DMSO- d_6): δ (ppm) 11.77 (s, 1H), 9.40 (s, 1H), 8.28 (s, 1H), 7.98 (d, J = 9.0 Hz, 2H), 7.72 (d, J = 8.7 Hz, 2H), 7.24 (dd, J = 3.5, 2.3 Hz, 1H), 7.14 (t, J = 9.1 Hz, 4H), 6.79 (dd, J = 3.5, 1.9 Hz, 1H). ^{13}C NMR (75 MHz, DMSO- d_6): δ (ppm) 162.1, 154.3, 151.7, 151.6, 149.9, 138.4, 128.3 (q, J = 3.6 Hz, C-20–22), 125.2 (q, J = 271.7 Hz), 123.6 (q, J = 32.1 Hz, 123.1, 122.7, 121.4, 118.0, 104.5, 99.6. Anal. Calcd for $C_{19}H_{13}F_3N_4O$: C, 61.62; H, 3.54; N, 15.13. Found: C, 61.55; H, 3.51; N, 15.04.

N-(4-(4-Bromophenoxy)phenyl)-7H-pyrrolo[2,3-d]pyrimidin-4-amine (34). Yield 83%. Mp 257–258 °C. 1H NMR (300 MHz, DMSO- d_6): δ (ppm) 11.75 (s, 1H), 9.35 (s, 1H), 8.27 (s, 1H), 7.93 (d, J = 9.0 Hz, 2H), 7.54 (d, J = 9.0 Hz, 2H), 7.24 (dd, J = 3.5, 2.3 Hz, 1H), 7.08 (d, J = 9.0 Hz, 2H), 6.96 (d, J = 8.9 Hz, 2H), 6.78 (dd, J = 3.5, 1.9 Hz, 1H). ^{13}C NMR (75 MHz, DMSO- d_6): δ (ppm) 157.7, 153.9, 151.3, 151.2, 150.6, 137.3, 133.1, 122.6, 122.4, 120.2, 120.1, 114.7, 104.0, 99.2. Anal. Calcd for $C_{18}H_{13}BrN_4O$: C, 56.71; H, 3.44; N, 14.70. Found: C, 56.21; H, 3.51; N, 14.43.

N-(4-(4-Nitrophenoxy)phenyl)-7H-pyrrolo[2,3-d]pyrimidin-4-amine (35). Yield 83%. Mp 270–271 °C. 1H NMR (300 MHz, DMSO- d_6): δ (ppm) 11.86 (s, 1H), 9.63 (s, 1H), 8.35–8.16 (m, 3H), 8.00 (d, J = 9.0 Hz, 2H), 7.29–7.24 (m, 1H), 7.20 (d, J = 9.0 Hz, 2H), 7.14 (d, J = 9.3 Hz, 2H), 6.84 (dd, J = 3.5, 1.9 Hz, 1H). ^{13}C NMR (75 MHz, DMSO- d_6): δ (ppm) 163.6, 153.1, 150.5, 150.1, 148.7, 142.0, 137.7, 126.2, 122.5, 122.3, 120.9, 116.9, 103.6, 99.1. ESI: calcd for $C_{18}H_{13}N_5O_3$ [M + H]⁺ 348.1091. Found: 348.1088

N-(4-(4-Aminophenoxy)phenyl)-7H-pyrrolo[2,3-d]pyrimidin-4-amine (36). Reduction of derivative 35 (1 equiv) using SnCl₂ (5.5 equiv) in EtOH (12 mL) at 100 °C for 20 min under microwave irradiation. Yield 9%. Mp 242–243 °C. 1H NMR (300 MHz, DMSO- d_6): δ (ppm) 11.68 (s, 1H), 9.21 (s, 1H), 8.21 (s, 1H), 7.75 (d, J = 9.0 Hz, 2H), 7.19 (dd, J = 3.5, 2.3 Hz, 1H), 6.87 (d, J = 9.0 Hz, 2H), 6.76 (d, J = 8.8 Hz, 2H), 6.71 (dd, J = 3.5, 1.9 Hz, 1H), 6.58 (d, J = 8.8 Hz, 2H), 4.92 (s, 2H). ^{13}C NMR (75 MHz, DMSO- d_6): δ (ppm) 153.74, 153.64, 150.8, 150.7, 146.5, 145.1, 134.7, 122.1, 121.9, 120.3, 117.0, 114.8, 103.3, 98.7. ESI: calcd for $C_{18}H_{15}N_5O$ [M + H]⁺ 318.1349. Found: 318.1348

N-(4-(p-Tolyl)phenyl)-7H-pyrrolo[2,3-d]pyrimidin-4-amine (37). Yield 57%. Mp 229 °C. 1H NMR (300 MHz, DMSO- d_6): δ (ppm) 11.72 (s, 1H), 9.29 (s, 1H), 8.24 (s, 1H), 7.85 (d, J = 9.0 Hz,

2H), 7.22 (dd, J = 3.5, 2.4 Hz, 1H), 7.17 (dd, J = 8.8, 0.7 Hz, 2H), 6.99 (d, J = 9 Hz, 2H), 6.89 (d, J = 8.5 Hz, 2H), 6.75 (dd, J = 3.5, 1.9 Hz, 1H), 2.28 (s, 3H). ^{13}C NMR (75 MHz, DMSO- d_6): δ (ppm) 155.2, 153.5, 151.5, 150.8, 136.0, 131.9, 130.3, 122.03, 121.98, 118.9, 117.9, 103.5, 98.7, 20.2. Anal. Calcd for $C_{19}H_{16}N_4O$: C, 72.13; H, 5.10; N, 17.71. Found: C, 71.84; H, 5.15; N, 17.96.

(4-(m-Tolyl)phenyl)-7H-pyrrolo[2,3-d]pyrimidine-2,4-diamine (38). Yield 80%. Mp 212–213 °C. 1H NMR (300 MHz, DMSO- d_6): δ (ppm) 11.73 (s, 1H), 9.31 (s, 1H), 8.25 (s, 1H), 7.88 (d, J = 9.0 Hz, 2H), 7.28–7.20 (m, 2H), 7.02 (d, J = 9.0 Hz, 2H), 6.91 (ddt, J = 7.5, 1.7, 0.8 Hz, 1H), 6.82–6.78 (m, 3H), 2.28 (s, 3H). ^{13}C NMR (75 MHz, DMSO- d_6): δ (ppm) 157.7, 153.5, 150.9, 150.79, 150.76, 139.6, 136.3, 129.6, 123.5, 122.1, 121.9, 119.4, 118.1, 114.7, 103.5, 98.7, 21.0. ESI: calcd for $C_{19}H_{16}N_4O$ [M + H]⁺ 317.1397. Found: 317.1393

N-(4-(3-Chlorophenoxy)phenyl)-7H-pyrrolo[2,3-d]pyrimidin-4-amine (39). Yield 62%. Mp 224–225 °C. 1H NMR (300 MHz, DMSO- d_6): δ (ppm) 11.79 (s, 1H), 9.39 (s, 1H), 8.29 (s, 1H), 7.96 (d, J = 9.0 Hz, 2H), 7.41 (t, J = 8.1 Hz, 1H), 7.26 (dd, J = 3.5, 2.2 Hz, 1H), 7.17 (ddd, J = 8.0, 2.0, 0.9 Hz, 1H), 7.12 (d, J = 9.0 Hz, 2H), 7.03 (t, J = 2.2 Hz, 1H), 6.97 (ddd, J = 8.3, 2.3, 0.8 Hz, 1H), 6.80 (dd, J = 3.5, 1.8 Hz, 1H). ^{13}C NMR (75 MHz, DMSO- d_6): δ (ppm) 158.9, 153.4, 150.8, 150.8, 149.7, 137.1, 133.9, 131.4, 122.5, 122.2, 121.9, 120.0, 117.2, 116.0, 103.5, 98.7. Anal. Calcd for $C_{18}H_{13}ClN_4O$: C, 64.20; H, 3.89; N, 16.64. Found: C, 64.06; H, 3.91; N, 16.75.

N-(4-(3-Trifluoromethylphenoxy)phenyl)-7H-pyrrolo[2,3-d]pyrimidin-4-amine (40). Yield 78%. Mp 176–177 °C. 1H NMR (300 MHz, DMSO- d_6): δ (ppm) 11.75 (s, 1H), 9.37 (s, 1H), 8.27 (s, 1H), 7.96 (d, J = 9.0 Hz, 2H), 7.61 (t, J = 7.8 Hz, 1H), 7.44 (d, J = 7.9 Hz, 1H), 7.32–7.19 (m, 3H), 7.13 (d, J = 8.9 Hz, 2H), 6.78 (dd, J = 3.5, 1.9 Hz, 1H). ^{13}C NMR (75 MHz, DMSO- d_6): δ (ppm) 158.8, 153.8, 151.2, 151.1, 149.9, 137.6, 131.6, 130.95 (q, J = 32 Hz), 127.7 (d, J = 272.5 Hz), 122.5, 122.3, 121.5, 120.5, 119.5 (d, J = 3.9 Hz), 113.9 (d, J = 4.0 Hz), 103.9, 99.1. Anal. Calcd for $C_{19}H_{13}F_3N_4O$: C, 61.62; H, 3.54; N, 15.13. Found: C, 61.06; H, 3.47; N, 15.22.

N-(4-(3-Methoxyphenoxy)phenyl)-7H-pyrrolo[2,3-d]pyrimidin-4-amine (41). Yield 33%. Mp 206–207 °C. 1H NMR (300 MHz, DMSO- d_6): δ (ppm) 11.73 (s, 1H), 9.32 (s, 1H), 8.25 (s, 1H), 7.89 (d, J = 9.0 Hz, 2H), 7.31–7.20 (m, 2H), 7.05 (d, J = 9.0 Hz, 2H), 6.76 (dd, J = 3.5, 1.8 Hz, 1H), 6.67 (ddd, J = 8.3, 2.4, 0.9 Hz, 1H), 6.59–6.48 (m, 2H), 3.73 (s, 3H). ^{13}C NMR (75 MHz, DMSO- d_6): δ (ppm) 160.6, 158.9, 153.5, 150.80, 150.75, 150.5, 136.5, 130.4, 122.1, 121.9, 119.6, 109.5, 108.4, 103.7, 103.5, 98.7, 55.2. ESI: calcd for $C_{19}H_{16}NO_2$ [M + H]⁺ 333.1342. Found: 333.1342.

N-(4-(2-Chlorophenoxy)phenyl)-7H-pyrrolo[2,3-d]pyrimidin-4-amine (42). Yield 79%. Mp 214–215 °C. 1H NMR (300 MHz, DMSO- d_6): δ (ppm) 11.73 (s, 1H), 9.33 (s, 1H), 8.25 (s, 1H), 7.89 (d, J = 9.0 Hz, 2H), 7.58 (dd, J = 8.0, 1.6 Hz, 1H), 7.34 (ddd, J = 8.2, 7.4, 1.6 Hz, 1H), 7.22 (dd, J = 3.5, 2.4 Hz, 1H), 7.17 (ddd, J = 8.0, 7.4, 1.5 Hz, 1H), 7.05–6.95 (m, 3H), 6.76 (dd, J = 3.5, 1.9 Hz, 1H). ^{13}C NMR (75 MHz, DMSO- d_6): δ (ppm) 153.5, 152.6, 150.80, 150.74, 150.71, 136.5, 130.6, 128.7, 124.6, 123.8, 122.1, 122.0, 119.8, 118.4, 103.5, 98.7. Anal. Calcd for $C_{18}H_{13}ClN_4O$: C, 64.20; H, 3.89; N, 16.64. Found: C, 64.11; H, 3.96; N, 16.63.

N-(4-(2-Methoxyphenoxy)phenyl)-7H-pyrrolo[2,3-d]pyrimidin-4-amine (43). Yield 64%. Mp 214–215 °C. 1H NMR (300 MHz, DMSO- d_6): δ (ppm) 11.69 (s, 1H), 9.23 (s, 1H), 8.21 (s, 1H), 7.76 (d, J = 9.0 Hz, 2H), 7.20 (dd, J = 3.5, 2.3 Hz, 1H), 7.18–7.14 (m, 2H), 7.02–6.92 (m, 2H), 6.86 (d, J = 9.1 Hz, 2H), 6.71 (dd, J = 3.5, 1.9 Hz, 1H), 3.77 (s, 3H). ^{13}C NMR (75 MHz, DMSO- d_6): δ (ppm) 153.6, 152.6, 151.1, 150.8, 150.7, 144.6, 135.0, 124.9, 122.1, 121.9, 121.0, 120.7, 116.7, 113.3, 103.3, 98.7, 55.6. Anal. Calcd for $C_{19}H_{16}NO_2$: C, 68.66; H, 4.85; N, 16.96. Found: C, 68.60; H, 4.82; N, 16.97.

N-(4-(2,4-Chlorophenoxy)phenyl)-7H-pyrrolo[2,3-d]pyrimidin-4-amine (44). Yield 63%. Mp 252–253 °C. 1H NMR (300 MHz, DMSO- d_6): δ (ppm) 11.72 (s, 1H), 9.37 (s, 1H), 8.24 (s, 1H), 7.89 (d, J = 9.1 Hz, 2H), 7.72 (d, J = 2.5 Hz, 1H), 7.39 (dd, J = 8.8, 2.6 Hz, 1H), 7.22 (dd, J = 3.5, 2.3 Hz, 1H), 7.02 (dd, J = 8.9, 2.1 Hz, 3H), 6.75 (dd, J = 3.5, 1.9 Hz, 1H). ^{13}C NMR (75 MHz, DMSO- d_6): δ (ppm) 153.6, 152.0, 150.9, 150.5, 136.9, 130.1, 128.8, 127.7, 124.9,

122.4, 122.2, 120.9, 118.8, 103.7, 98.9. Anal. Calcd for $C_{18}H_{12}Cl_2N_4O$: C, 58.24; H, 3.26; N, 15.09. Found: C, 58.13; H, 3.33; N, 15.17.

N4-(4-(4-Chlorophenoxy)phenyl)-7H-pyrrolo[2,3-d]pyrimidine-2,4-diamine (45). Yield 70%. Mp 232–233 °C. 1H NMR (300 MHz, DMSO- d_6): δ (ppm) 10.83 (s, 1H), 8.94 (s, 1H), 7.98 (d, J = 9.1 Hz, 2H), 7.41 (d, J = 9.0 Hz, 2H), 6.99 (m, 4H), 6.76 (dd, J = 3.5, 2.1 Hz, 1H), 6.53 (dd, J = 3.5, 1.9 Hz, 1H), 5.70 (s, 2H). ^{13}C NMR (75 MHz, DMSO- d_6): δ (ppm) 159.4, 156.8, 154.0, 153.5, 149.7, 137.5, 129.7, 126.3, 121.3, 119.5, 119.1, 117.8, 98.8, 96.9. ESI: calcd for $C_{18}H_{14}ClN_5O$ [M + H]⁺ 352.0960. Found: 352.0956.

N4-(4-(4-(Trifluoromethyl)phenoxy)phenyl)-7H-pyrrolo[2,3-d]pyrimidine-2,4-diamine (46). Yield 77%. Mp 201–202 °C. 1H NMR (300 MHz, DMSO- d_6): δ (ppm) 10.85 (s, 1H), 8.99 (s, 1H), 8.03 (d, J = 9.0 Hz, 2H), 7.72 (d, J = 9.0 Hz, 2H), 7.11 (dd, J = 9.0, 0.8 Hz, 2H), 7.07 (d, J = 9.0 Hz, 2H), 6.77 (dd, J = 3.5, 2.2 Hz, 1H), 6.55 (dd, J = 3.5, 1.9 Hz, 1H), 5.72 (s, 2H). ^{13}C NMR (75 MHz, DMSO- d_6): δ (ppm) 161.3, 159.4, 153.9, 153.5, 148.5, 138.2, 127.4 (q, J = 3.7 Hz), 124.4 (d, J = 271.1 Hz), 122.7 (d, J = 32 Hz), 121.2, 120.4, 117.9, 117.1, 108.5, 98.8, 96.9. ESI: calcd for $C_{19}H_{14}F_3N_5O$ [M + H]⁺ 386.1223. Found: 386.1220.

N4-(4-(3-Chlorophenoxy)phenyl)-7H-pyrrolo[2,3-d]pyrimidine-2,4-diamine (47). Yield 16%. Mp 177–178 °C. 1H NMR (300 MHz, DMSO- d_6): δ (ppm) 10.84 (s, 1H), 8.97 (s, 1H), 8.00 (d, J = 9.0 Hz, 2H), 7.39 (t, J = 8.1 Hz, 1H), 7.14 (ddd, J = 8.0, 2.0, 0.9 Hz, 1H), 7.03 (d, J = 9.0 Hz, 2H), 6.99 (t, J = 2.2 Hz, 1H), 6.94 (ddd, J = 8.3, 2.4, 0.9 Hz, 1H), 6.76 (dd, J = 3.5, 2.2 Hz, 1H), 6.54 (dd, J = 3.5, 1.9 Hz, 1H), 5.71 (s, 2H). ^{13}C NMR (75 MHz, DMSO- d_6): δ (ppm) 159.4, 159.1, 153.9, 153.5, 149.1, 137.8, 133.9, 131.3, 122.5, 121.3, 119.9, 117.8, 117.1, 116.0, 98.8, 96.9. ESI: calcd for $C_{18}H_{14}ClN_5O$ [M + H]⁺ 352.0960. Found: 352.0955.

N4-(4-(3-(Trifluoromethyl)phenoxy)phenyl)-7H-pyrrolo[2,3-d]pyrimidine-2,4-diamine (48). Yield 45%. Mp 179–180 °C. 1H NMR (300 MHz, DMSO- d_6): δ (ppm) 10.84 (s, 1H), 8.98 (s, 1H), 8.02 (d, J = 9.1 Hz, 2H), 7.60 (t, J = 7.9 Hz, 1H), 7.44 (ddt, J = 7.7, 1.7, 0.9 Hz, 1H), 7.32–7.20 (m, 2H), 7.06 (d, J = 9.0 Hz, 2H), 6.76 (dd, J = 3.5, 2.2 Hz, 1H), 6.54 (dd, J = 3.5, 2.0 Hz, 1H), 5.72 (s, 2H). ^{13}C NMR (75 MHz, DMSO- d_6): δ (ppm) 159.4, 158.6, 153.9, 153.5, 148.9, 138.0, 131.3, 130.6 (d, J = 31.9 Hz), 123.8 (d, J = 272.5 Hz), 121.3, 121.1, 120.0, 119.0 (d, J = 4.1 Hz), 117.9, 113.4 (d, J = 4.0 Hz), 98.8, 96.9. ESI: calcd for $C_{19}H_{14}F_3N_5O$ [M + H]⁺ 386.1223. Found: 386.1219.

N-(4-(4-Nitrophenyl)thio)phenyl)-7H-pyrrolo[2,3-d]pyrimidin-4-amine (49). Yield 42%. Mp 265–266 °C. 1H NMR (300 MHz, DMSO- d_6): δ (ppm) 12.46 (s, 1H), 10.72 (s, 1H), 8.43 (s, 1H), 8.17 (d, J = 8.6 Hz, 2H), 8.00 (d, J = 8.1 Hz, 2H), 7.67 (d, J = 8.2 Hz, 2H), 7.44 (t, J = 2.6 Hz, 1H), 7.33 (d, J = 8.6 Hz, 2H), 7.03 (t, J = 2.4 Hz, 1H). ^{13}C NMR (75 MHz, DMSO- d_6): δ (ppm) 151.7, 148.3, 147.6, 146.6, 144.9, 139.9, 135.7, 126.4, 124.3, 124.1, 123.7, 123.5, 103.7, 100.7. Anal. Calcd for $C_{18}H_{13}N_5O_2S$: C, 59.49; H, 3.61; N, 19.27; S, 8.82. Found: C, 59.42; H, 3.78; N, 19.14; S, 8.74.

N-(4-(4-Aminophenyl)thio)phenyl)-7H-pyrrolo[2,3-d]pyrimidin-4-amine (50). Reduction of derivative 49 (1 equiv) using $SnCl_2$ (5.5 equiv) in EtOH (12 mL) at 100 °C for 20 min under microwave irradiation. Yield 69%. Mp 200–201 °C. 1H NMR (300 MHz, DMSO- d_6): δ (ppm) 11.73 (s, 1H), 9.30 (s, 1H), 8.24 (s, 1H), 7.80 (d, J = 8.8 Hz, 2H), 7.23 (dd, J = 3.5, 2.3 Hz, 1H), 7.22 (dd, J = 3.5, 2.3 Hz, 1H), 7.14 (dd, J = 16.7, 8.6 Hz, 4H), 6.84 (dd, J = 3.5, 1.9 Hz, 1H), 6.61 (d, J = 8.5 Hz, 2H), 5.48 (s, 1H). ^{13}C NMR (75 MHz, DMSO- d_6): δ (ppm) 153.3, 150.8, 150.6, 149.3, 138.5, 135.0, 131.3, 128.2, 122.1, 120.9, 117.1, 114.7, 103.6, 98.7. Anal. Calcd for $C_{18}H_{15}N_5S$: C, 59.49; H, 3.61; N, 19.27; S, 8.82. Found: C, 59.26; H, 3.70; N, 19.37; S, 8.95.

N-(Benzyl oxy)phenyl)-7H-pyrrolo[2,3-d]pyrimidin-4-amine (51). Yield 28%. Mp 238–239 °C. 1H NMR (300 MHz, DMSO- d_6): δ (ppm) 11.66 (s, 1H), 9.15 (s, 1H), 8.20 (s, 1H), 7.71 (d, J = 9.1 Hz, 2H), 7.50–7.29 (m, 5H), 7.18 (dd, J = 3.5, 2.4 Hz, 1H), 7.00 (d, J = 9.1 Hz, 2H), 6.67 (dd, J = 3.5, 1.9 Hz, 1H), 5.09 (s, 2H). ^{13}C NMR (75 MHz, DMSO- d_6): δ (ppm) 153.80, 153.76, 150.9, 150.7, 137.3,

133.5, 128.4, 127.74, 127.66, 122.3, 122.0, 114.7, 103.2, 98.7, 69.4. ESI: calcd for $C_{19}H_{16}N_4O$ [M + H]⁺ 317.1397. Found: 317.1395.

(4-((7H-Pyrrolo[2,3-d]pyrimidin-4-yl)amino)phenyl)(phenyl)methanone (52). Yield 97%. Mp 247–248 °C. 1H NMR (300 MHz, DMSO- d_6): δ (ppm) 11.91 (s, 1H), 9.76 (s, 1H), 8.38 (s, 1H), 8.16 (d, J = 8.9 Hz, 2H), 7.79 (d, J = 8.8 Hz, 2H), 7.77–7.53 (m, 5H), 7.32 (dd, J = 3.5, 2.3 Hz, 1H), 6.89 (dd, J = 3.5, 1.9 Hz, 1H). ^{13}C NMR (75 MHz, DMSO- d_6): δ (ppm) 194.4, 152.8, 151.2, 150.5, 145.1, 137.9, 132.0, 131.1, 129.6, 129.3, 128.4, 123.0, 118.6, 104.4, 98.7. ESI: calcd for $C_{19}H_{14}N_4O$ [M + H]⁺ 315.1240. Found: 315.1238.

(4-((7H-Pyrrolo[2,3-d]pyrimidin-4-yl)amino)phenyl)(4-fluorophenyl)methanone (53). Yield 19%. Mp 275–276 °C. 1H NMR (300 MHz, DMSO- d_6): δ (ppm) 11.89 (s, 1H), 9.75 (s, 1H), 8.38 (s, 1H), 8.16 (d, J = 8.9 Hz, 2H), 7.93–7.72 (m, 4H), 7.39 (t, J = 8.9 Hz, 2H), 7.32 (dd, J = 3.5, 2.3 Hz, 1H), 6.88 (dd, J = 3.5, 2.3, 1H). ^{13}C NMR (75 MHz, DMSO- d_6): δ (ppm) 193.1, 164.3 (d, J = 250.3 Hz, 152.9, 151.2, 150.5, 145.2, 134.5 (d, J = 3.2 Hz), 132.2 (d, J = 9.2 Hz), 131.1, 129.5, 123.0, 118.7, 115.5 (d, J = 22.0 Hz), 104.4, 98.8. Anal. Calcd for $C_{19}H_{13}FN_4O$: C, 68.67; H, 3.94; N, 16.86. Found: C, 68.32; H, 3.90; N, 16.72.

(4-((7H-Pyrrolo[2,3-d]pyrimidin-4-yl)amino)phenyl)(3,4-dichlorophenyl)methanone (54). Yield 35%. Mp 274–275 °C. 1H NMR (300 MHz, DMSO- d_6): δ (ppm) 11.91 (s, 1H), 9.78 (s, 1H), 8.39 (s, 1H), 8.18 (d, J = 8.9 Hz, 2H), 7.91 (d, J = 1.9 Hz, 1H), 7.82 (dd, J = 8.5, 6.3 Hz, 3H), 7.68 (dd, J = 8.3, 2.0 Hz, 1H), 7.33 (dd, J = 3.5, 2.3 Hz, 1H), 6.88 (dd, J = 3.5, 1.9 Hz, 1H). ^{13}C NMR (75 MHz, DMSO- d_6): δ (ppm) 192.0, 152.8, 151.2, 150.5, 145.6, 138.4, 134.6, 131.5, 131.3, 130.9, 130.8, 129.3, 128.7, 123.1, 118.7, 104.5, 98.7. ESI: calcd for $C_{19}H_{12}Cl_2N_4O$ [M + H]⁺ 383.0461. Found: 383.0457

N-(4-(Pyridin-3-yloxy)phenyl)-7H-pyrrolo[2,3-d]pyrimidin-4-amine (55). Yield 35%. Mp 203–204 °C. 1H NMR (300 MHz, DMSO- d_6): δ (ppm) 11.75 (s, 1H), 9.36 (s, 1H), 8.40–8.36 (m, 1H), 8.35–8.31 (m, 1H), 8.26 (s, 1H), 7.93 (d, J = 9.0 Hz, 2H), 7.45–7.36 (m, 2H), 7.23 (dd, J = 3.5, 2.3 Hz, 1H), 7.10 (d, J = 9.0 Hz, 2H), 6.77 (dd, J = 3.5, 1.9 Hz, 1H). ^{13}C NMR (75 MHz, DMSO- d_6): δ (ppm) 154.2, 153.5, 150.82, 150.74, 150.1, 143.9, 140.2, 137.0, 124.60, 124.55, 122.2, 121.9, 119.5, 103.6, 98.7. ESI: calcd for $C_{17}H_{13}N_5O$ [M + H]⁺ 304.11193. Found: 304.11191.

Procedure for the Synthesis of Azides Derivatives 56–60. First, 1 equiv of 1-(bromomethyl) or 1-(bromoethyl)benzene and 1.5 equiv of sodium azide were dissolved in 2 mL of DMF. The reaction mixture was stirred overnight. The organic phase (AcOEt, 10 mL) was washed with 10 × 3 mL of iced H_2O . The organic phase was dried over Na_2SO_4 , and the crude was used in the following reaction without further purification.

1-(Azydomethyl)-4-chlorobenzene (56). Yield 74%. 1H NMR (300 MHz, DMSO- d_6): δ (ppm) 7.47 (d, J = 8.6 Hz, 2H), 7.42 (d, J = 8.7 Hz, 2H), 4.47 (s, 2H). ^{13}C NMR (75 MHz, DMSO- d_6): δ (ppm) 135.2, 133.2, 130.8, 129.2, 53.2.

1-(Azydomethyl)-2-chlorobenzene (57). Yield 65%. 1H NMR (300 MHz, DMSO- d_6): δ (ppm) 7.46–7.35 (m, 2H), 7.33–7.24 (m, 2H), 4.50 (s, 2H). ^{13}C NMR (75 MHz, DMSO- d_6): δ (ppm) 133.8, 133.3, 130.0, 129.8, 129.6, 127.2, 52.3.

1-(Azydomethyl)-3-chlorobenzene (58). Yield 84%. 1H NMR (300 MHz, DMSO- d_6): δ (ppm) 7.32 (dd, J = 3.8, 0.8 Hz, 3H), 7.25–7.12 (m, 1H), 4.33 (s, 2H). ^{13}C NMR (75 MHz, DMSO- d_6): δ (ppm) 137.5, 134.9, 130.3, 128.6, 128.3, 126.3, 54.3.

2-Azydoethylbenzene (59). Yield 53%. 1H NMR (300 MHz, DMSO- d_6): δ (ppm) 7.35–7.18 (m, 5H), 3.56 (t, J = 7.1 Hz, 2H), 2.85 (t, J = 7.1 Hz, 2H). ^{13}C NMR (75 MHz, DMSO- d_6): δ (ppm) 138.8, 129.3, 128.9, 126.9, 52.0, 34.9.

1-(Azidomethyl)-4-methylbenzene (60). Yield 56%. 1H NMR (300 MHz, DMSO- d_6): δ (ppm) 7.34–7.15 (m, 4H), 4.38 (s, 2H), 2.31 (s, 3H). ^{13}C NMR (75 MHz, DMSO- d_6): δ (ppm) 137.2, 133.0, 129.8, 128.0, 52.2, 21.6.

N-(Prop-2-yn-1-yloxy)phenyl)-7H-pyrrolo[2,3-d]pyrimidin-4-amine (61). Synthesized following procedure a. Yield 69%. Mp 217–218 °C. 1H NMR (300 MHz, DMSO- d_6): δ (ppm) 11.70 (s, 1H), 9.19 (s, 1H), 8.21 (s, 1H), 7.74 (dt, J = 9.5, 3.4 Hz, 2H), 7.19 (dd, J =

3.5, 2.3 Hz, 1H), 6.98 (dd, J = 9.0, 3.4 Hz, 2H), 6.70 (dd, J = 3.5, 1.9 Hz, 1H), 4.77 (d, J = 2.4 Hz, 2H), 3.57 (t, J = 2.3 Hz, 1H). ^{13}C NMR (75 MHz, DMSO- d_6): δ (ppm) 153.7, 152.6, 150.8, 150.7, 134.0, 122.1, 121.8, 114.8, 103.2, 98.7, 79.5, 78.1, 55.6. Anal. Calcd for $\text{C}_{15}\text{H}_{12}\text{N}_4\text{O}$: C, 68.17; H, 4.58; N, 21.20. Found: C, 67.86; H, 4.63; N, 21.23.

Procedure for the Synthesis of Triazol Derivatives 62–67. A mixture of compound **61** (1 equiv) and the corresponding azide (1 equiv) in DMF was reacted overnight at r.t. in the presence of copper sulfate ($\text{CuSO}_4 \cdot 5\text{H}_2\text{O}$) (0.1 equiv), tris(benzyltriazolylmethyl)amine (TBTA) (0.1 equiv), and sodium ascorbate (0.2 equiv). The reaction mixture was poured onto water, extracted with $\text{CH}_2\text{Cl}_2/\text{MeOH}$ (9:1), washed with saturated sodium chloride solution, dried over magnesium sulfate (MgSO_4), concentrated, and purified using flash chromatography on silica gel ($\text{CH}_2\text{Cl}_2/\text{MeOH}$ mixture).

N-(4-((1-p-Phenyl-1H-1,2,3-triazol-4-yl)methoxy)phenyl)-7H-pyrrolo[2,3-d]pyrimidin-4-amine (62). Yield 34%. Mp 267–268 °C. ^1H NMR (500 MHz, DMSO- d_6): δ (ppm) 11.68 (s, 1H), 9.18 (s, 1H), 8.97 (s, 1H), 8.22 (s, 1H), 7.92 (dd, J = 7.0, 1.5 Hz, 2H), 7.76 (d, J = 9.0 Hz, 2H), 7.61 (t, J = 7.9 Hz, 2H), 7.50 (t, J = 7.5, 1.0 Hz, 1H), 7.19 (dd, J = 3.5, 2.2 Hz, 1H), 7.08 (d, J = 9.1, 2H), 6.70 (dd, J = 3.5, 1.8 Hz, 1H), 5.23 (s, 2H). ^{13}C NMR (125 MHz, DMSO- d_6): δ (ppm) 153.7, 153.4, 150.9, 150.7, 144.1, 136.6, 133.8, 129.9, 122.8, 122.2, 121.8, 120.1, 114.7, 103.3, 98.8, 61.3. ESI: calcd for $\text{C}_{21}\text{H}_{17}\text{N}_3\text{O}$ [M + H]⁺ 384.1567. Found: 384.1564.

N-(4-((1-(4-Chlorobenzyl)-1H-1,2,3-triazol-4-yl)methoxy)phenyl)-7H-pyrrolo[2,3-d]pyrimidin-4-amine (63). Yield 64%. Mp 207–208 °C. ^1H NMR (300 MHz, DMSO- d_6): δ (ppm) 11.67 (s, 1H), 9.16 (s, 1H), 8.29 (s, 1H), 8.20 (s, 1H), 7.73 (d, J = 9.1 Hz, 2H), 7.45 (d, J = 8.5 Hz, 2H), 7.35 (d, J = 8.5 Hz, 2H), 7.18 (dd, J = 3.5, 2.3 Hz, 1H), 7.01 (d, J = 9.1 Hz, 2H), 6.68 (dd, J = 3.5, 1.8 Hz, 1H), 5.62 (s, 2H), 5.12 (s, 2H). ^{13}C NMR (75 MHz, DMSO- d_6): δ (ppm) 153.7, 153.4, 150.9, 150.7, 143.3, 135.0, 133.7, 132.9, 129.9, 128.8, 124.7, 122.2, 121.8, 114.7, 112.2, 98.8, 61.3, 52.0. ESI: calcd for $\text{C}_{22}\text{H}_{18}\text{N}_3\text{O}$ [M + H]⁺ 432.1334. Found: 432.1320.

N-(4-((1-(2-Chlorobenzyl)-1H-1,2,3-triazol-4-yl)methoxy)phenyl)-7H-pyrrolo[2,3-d]pyrimidin-4-amine (64). Yield 31%. Mp 173–174 °C. ^1H NMR (500 MHz, DMSO- d_6): δ (ppm) 11.67 (s, 1H), 9.16 (s, 1H), 8.27 (s, 1H), 8.21 (s, 1H), 7.73 (d, J = 9.0 Hz, 2H), 7.53 (dd, J = 7.5, 1.7 Hz, 1H), 7.39 (dd, J = 7.4, 1.7 Hz, 2H), 7.22 (dd, J = 7.3, 2.1 Hz, 1H), 7.18 (dd, J = 3.4, 2.3 Hz, 1H), 7.02 (d, J = 9.0 Hz, 2H), 6.68 (dd, J = 3.4, 1.9 Hz, 1H), 5.73 (s, 2H), 5.13 (s, 2H). ^{13}C NMR (125 MHz, DMSO- d_6): δ (ppm) 153.7, 153.4, 150.9, 150.7, 143.0, 133.7, 133.3, 132.6, 130.5, 130.2, 129.6, 127.7, 125.0, 122.2, 121.8, 114.7, 103.2, 98.7, 61.3, 50.6. ESI: calcd for $\text{C}_{22}\text{H}_{18}\text{N}_3\text{O}$ [M + H]⁺ 432.1334. Found: 432.1337.

N-(4-((1-(3-Chlorobenzyl)-1H-1,2,3-triazol-4-yl)methoxy)phenyl)-7H-pyrrolo[2,3-d]pyrimidin-4-amine (65). Yield 33%. mp 177–178 °C. ^1H NMR (500 MHz, DMSO- d_6): δ (ppm) 11.67 (s, 1H), 9.15 (s, 1H), 8.33 (s, 1H), 8.20 (s, 1H), 7.73 (d, J = 9.1 Hz, 2H), 7.41 (d, J = 3.1 Hz, 3H), 7.32–7.25 (m, 1H), 7.18 (dd, J = 3.4, 2.3 Hz, 1H), 7.02 (d, J = 9.0 Hz, 2H), 6.68 (dd, J = 3.5, 1.9 Hz, 1H), 5.64 (s, 2H), 5.33 (s, 2H). ^{13}C NMR (125 MHz, DMSO- d_6): δ (ppm) 153.7, 53.4, 150.9, 150.7, 143.3, 138.4, 133.7, 133.3, 130.7, 128.1, 127.9, 126.7, 124.8, 122.2, 121.8, 114.7, 103.2, 98.7. ESI: calcd for $\text{C}_{22}\text{H}_{18}\text{N}_3\text{O}$ [M + H]⁺ 432.1334. Found: 432.1328.

N-(4-((1-Phenethyl)-1H-1,2,3-triazol-4-yl)methoxy)phenyl)-7H-pyrrolo[2,3-d]pyrimidin-4-amine (66). Yield 64%. Mp 206–207 °C. ^1H NMR (500 MHz, DMSO- d_6): δ (ppm) 11.67 (s, 1H), 9.16 (s, 1H), 8.21 (s, 1H), 8.16 (s, 1H), 7.73 (d, J = 9.1 Hz, 2H), 7.30–7.16 (m, 6H), 7.00 (d, J = 9.1 Hz, 2H), 6.69 (dd, J = 3.5, 2.1 Hz, 1H), 5.10 (s, 2H), 4.62 (t, J = 7.4 Hz, 2H), 3.17 (t, J = 7.4 Hz, 2H). ^{13}C NMR (125 MHz, DMSO- d_6): δ (ppm) 153.7, 153.4, 150.9, 150.7, 142.7, 142.7, 133.7, 128.7, 128.4, 126.6, 124.4, 122.2, 121.8, 114.7, 103.2, 98.7, 62.3, 50.5, 35.7. ESI: calcd for $\text{C}_{23}\text{H}_{21}\text{N}_3\text{O}$ [M + H]⁺ 412.1880. Found: 412.1873.

N-(4-((1-(4-Methylbenzyl)-1H-1,2,3-triazol-4-yl)methoxy)phenyl)-7H-pyrrolo[2,3-d]pyrimidin-4-amine (67). Yield 73%. Mp 215–216 °C. ^1H NMR (500 MHz, DMSO- d_6): δ (ppm) 11.67 (s, 1H), 9.15 (s, 1H), 8.24 (s, 1H), 8.20 (s, 1H), 7.72 (d, J = 9.0 Hz,

2H), 7.22 (d, J = 8.0 Hz, 2H), 7.20–7.15 (m, 3H), 7.00 (d, J = 9.0 Hz, 2H), 6.68 (d, J = 3.3 Hz, 1H), 5.55 (s, 2H), 5.11 (s, 2H), 2.27 (s, 3H). ^{13}C NMR (125 MHz, DMSO- d_6): δ (ppm) 153.7, 153.4, 150.9, 150.7, 143.1, 137.5, 133.7, 133.0, 129.3, 128.0, 124.6, 122.2, 121.8, 114.7, 103.2, 98.7, 61.3, 52.6, 20.7. ESI: calcd for $\text{C}_{23}\text{H}_{21}\text{N}_3\text{O}$ [M + H]⁺ 412.1880. Found: 412.1876

X-ray Diffraction Studies. Protein Expression and Purification.

The protein was expressed following the protocol by Xue et al.²⁴ In brief, the gene of human TTBK1 coding for the catalytic domain, residues from 14 to 313 (GeneScrip hTTBK_{coli}_pET-28a(+)-TEV), was expressed in *Escherichia coli* (BL21DE3). A preculture was grown overnight in LB medium, diluted 1:25 in fresh LB medium, and incubated at 37 °C with shaking until an OD₆₀₀ of 0.6 was reached. Induction was carried out using 1 mM IPTG at 20 °C overnight.

Harvested cells were resuspended in buffer A (20 mM Tris, pH 8.0, 5 mM MgCl₂, 300 mM NaCl, 5% (v/v) glycerol, 0.05% (w/v) CHAPS, and 1 mM tris(2-carboxyethyl)phosphine (TCEP), 10 mM imidazole) with an EDTA-free protease inhibitor cocktail (Roche) and lysed with a single passage through a cell disruptor (MIXONIX Inc.). The lysate was clarified by centrifugation, and the supernatant loaded onto a 1 mL HiTrap Crude column (GE Healthcare). After washing with 30 column volumes (CV) of buffer A, the protein was eluted with increasing concentrations of buffer A supplemented with 250 mM imidazole. Fractions containing TTBK1 were pooled, diluted threefold with buffer C (20 mM HEPES, pH 7.0, 5% (v/v) glycerol), and loaded onto a pre-equilibrated 10 mL Resource S column (GE Healthcare). The column was washed with 5 CV of buffer C, and the bound protein was eluted by a salt gradient with buffer C containing 1 M NaCl. Fractions containing TTBK1 were then loaded onto a Hiload 16/60 Superdex 200 pre-equilibrated with buffer D (20 mM Tris, pH 8.0, 0.5 mM MgCl₂, 300 mM NaCl, 5% (v/v) glycerol, 0.05% (w/v) CHAPS, and 2 mM TCEP). Finally, fractions containing TTBK1 were concentrated in Amicon Ultra centrifugal units (10 K MWCO) and snap frozen in liquid nitrogen. This protein was used for the **29**-complexed crystallization.

For the other crystal structures, TTBK1 (aa 13–320) and TTBK2 (aa 1–299) were recombinantly coexpressed with λ-phosphatase in *E. coli* Rosetta as a His-SumO- and His-tagged proteins, respectively. Both proteins were initially purified by Ni²⁺-affinity chromatography, and the tags were cleaved either by SENP1 protease (TTBK1) or TEV (TTBK2). The cleaved proteins were further purified by size exclusion chromatography, and the pure proteins were stored in buffer 25 mM HEPES pH 7.5, 250 mM NaCl, 0.5 mM TCEP, and 10% glycerol.

Crystallization. For derivative **29**, crystallization experiments were performed in pregreased 24-well plates (Crystalfgen Inc.) and reagents were purchased from commercial sources. The TEV-TTBK1(14–313) protein was used in crystallization. All TTBK1 crystals were obtained using the hanging drop technique at 20 °C by mixing 0.5 μL of protein (9.5 mg mL⁻¹) with 0.5 μL of the reservoir solution and were equilibrated against 1 mL of the reservoir solution. **29**–TTBK1 cocrystals were obtained by preincubating the protein with the compound in threefold-excess molar in a 27% (w/v) PEG 4000, 200 mM NH₄SO₄, 100 mM Na Citrate pH 5.6, and 10 mM TCEP solution. Needle-like crystals appeared after 1 week and grew until 50 μm in size. Crystals were transferred to a cryo solution consisting in the well solution plus 20% (v/v) ethylenglycol.

For other structures, crystallization was performed using sitting drop vapor diffusion at 20 °C and the kinases at a concentration of ~10 mg/mL that were preincubated with 1 mM inhibitors. For TTBK2, the crystallization condition was 1.6 M Na/K phosphate pH 7.0, 5% glycerol, and 0.1 M Tris pH 7.5–8.5, while for TTBK1 the condition was 26% PEG 3350, 0.2 M sodium acetate pH 7.0, and 0.1 M Tris, pH 7.5–8.5. The complexed crystals were cryo-protected with the mother liquor supplemented with glycerol or ethylene glycol for TTBK2 or TTBK1, respectively.

Structure Determination. Diffraction data for TTBK1-**29** were collected in the XALOC beamline at the ALBA synchrotron (Barcelona, Spain). For the other crystal structures, diffraction data were collected at the Swiss Light Source. The collected data sets were

processed with XDS⁴¹ and AIMLESS.⁴² Structure determination was performed by the molecular replacement method with PHASER⁴³ using the previously TTBK1 KD structure (PDB ID 4BTM). Structure refinement was done by several cycles of computational refinement with REFMAC5⁴⁴ and manual rebuilding using Coot.⁴⁵ Crystallographic data collection and refinement statistic are summarized in Table S1.

Computational Studies. The protein–ligand docking was performed using Glide and related Schrödinger packages.^{46,47} The binding site was defined by the crystallographic structures obtained for TTBK1 and TTBK2 in complex with the inhibitors reported in this work (PDB IDs 7Q8V, 7Q8W, 7Q8Z, 7Q90, and 7Q8Y). Before docking calculations, the protein was prepared using Maestro Protein Preparation Wizard⁴⁸ by removing ligands, metals, and water molecules; adding hydrogens; ionizing residues at pH 7.5; and filling in missing side chains using Prime. Minimization of the protein structure was done with OPLS3 force field. Inhibitors of the TTBKs were also prepared using OPLS force field to minimize energy. The grid box was defined using the ligands cocrystallized in TTBK1 and TTBK2 as the center of the boxes. The docking was performed with the Glide standard precision (SP) function,⁴⁹ and the top 10 poses per docked ligand were selected and subjected to rescoring with the molecular mechanics-generalized Born surface area (MM-GBSA) with Prime. This computational method combines molecular mechanics energy and implicit solvation models, which enable the docking results to be rescored and correlates the experimental activities (IC_{50}) with the predicted binding energies (ΔG_{bind}). The binding free energies between the ligands and the receptor were calculated as previously reported.¹⁵

The crystal structures of complexes 29–TTBK1, 42–TTBK1, and 42–TTBK2 as well as the best docking solutions between compound 38 and TTBK1 and TTBK2, which present the best predicted binding free energy (MM-GBSA), were subjected to 525 ns of molecular dynamics simulations (MDs) using Desmond software⁵⁰ and the OPLS3e force field.⁵¹ To prepare the systems, the complexes were solvated with pre-equilibrated SPC water molecules in a periodic boundary condition box. Then, the systems were neutralized by adding Na^+ or Cl^- counterions to balance the net charge of the systems. NaCl was added at a concentration of 0.15 M to simulate physiological conditions. Each system was relaxed using the default Desmond relaxation protocol and then equilibrated with a spring constant force of 5.0 kcal/(mol· \AA^2), which was applied to the backbone atoms of the TTBKs and the ligands for 25 ns using the NPT ensemble at constant pressure (1 atm), temperature (300 K), and number of atoms using the isothermal-isobaric ensemble and the Nosé–Hoover method with a relaxation time of 1 ps; the MTK algorithm was applied⁵² with a time step of 2 fs. Then, the last frame was taken, and a second nonrestricted 500 ns MDs was performed using the same conditions previously described. Systems were analyzed using the in house PyMol and VMD and a modification of the KNIME workflow to profile interactions between ligands and targets along MD trajectories.

Biology. *In Vitro Inhibition of TTBK1 and TTBK2 Human Recombinant Kinases.* The inhibition experiments were performed in the MRC Phosphorylation Unit (University of Dundee). TTBK1 or TTBK2 (human recombinant enzyme) (5–20 mU diluted in 50 mM Tris pH 7.5, 0.1 mM EGTA, 0.1% β -mercaptoethanol, 1 mg/mL BSA, and 10 mM DTT) was assayed against RRKDLHDDEEDEAMTSITA in a final volume of 25.5 μ L, which contained 50 mM Tris pH 7.5, 0.1 mM EGTA, 0.3 mM RRKDLHDDEEDEAMTSITA, 10 mM magnesium acetate, and 0.005 mM [^{33}P - γ -ATP] (50–1000 cpm/pmol). The mixture was incubated for 30 min at room temperature. Assays were stopped by addition of 5 μ L of 0.5 M (3%) orthophosphoric acid and then harvested onto P81 Unifilter plates with a wash buffer of 50 mM orthophosphoric acid.

Kinase Profiling. The kinase profiling studies were carried out by the MRC Phosphorylation Unit (University of Dundee) using the appropriate protocol in any case.⁵³

Parallel Artificial Membrane Permeability Assay (PAMPA) Blood–Brain Barrier (BBB). Prediction of the blood–brain barrier

penetration was done using the parallel artificial membrane permeability assay (PAMPA).⁵⁴ Ten commercial drugs of known BBB permeability, namely caffeine, enoxacine, hydrocortisone, desipramine, ofloxacin, piroxicam, testosterone, promazine, verapamil and atenolol, were used as controls in each experiment to validate the analysis set. Controls and TTBK1 inhibitors were dissolved in 5 mL of the experimental buffer (phosphate buffer saline solution at pH 7.4 (PBS)/EtOH (70:30 respectively)). The donor 96-well plate (Millipore, catalog no. MAIPS4510) was filled with 180 μ L of each filtered compound solution after being coated with 4 μ L of porcine brain lipid in dodecane (20 mg/mL) (Avanti Polar Lipids, catalog no. 141101). The acceptor 96-well plate (Millipore, catalog no. 141101) was filled with 180 μ L of the experimental buffer. Then, the donor plate was carefully put on the acceptor plate to form a “sandwich” for 2 h and 30 min at room temperature. During the incubation time, compounds diffused from the donor plate through the brain–lipid membrane into the acceptor plate. After incubation, the donor plate was removed, and the concentration of the compounds was determined in the acceptor and the donor plates by UV (Thermoscientific, Multiskan spectrum). Every sample was analyzed at 3–5 wavelengths in three wells and in two independent runs. Results are given as the mean \pm standard deviation (SD) of the two runs. Commercial drugs, PBS, ethanol, and dodecane were purchased from Sigma, Acros organics, Merck, Aldrich, and Fluka.

Cell Lines. All components for cell culture were obtained from Invitrogen (Barcelona, Spain). Antibodies used in this study are listed in Table S5.

Neuronal Cell Culture. Human neuroblastoma (SH-SY5Y) cells were purchased from the European Collection of Cell Cultures (Health Protection Agency, Salisbury, UK), and were propagated in Dulbecco's Modified Eagle Medium containing L-glutamine (2 mM), 1% nonessential amino acids, 10% fetal bovine serum, and 1% penicillin/streptomycin under humidified 5% CO₂ conditions at 37 °C. upon attaining semiconfluence, cells were pretreated with TTBK1 inhibitors (5 μ M) or the commercial GSK3 β inhibitor (Tideglusib, 5 μ M) and then exposed 1 h later to ethacrynic acid (40 μ M) for 24 h. After the incubation time, cultures were processed for the cell viability assay or Western blotting analysis. Cell viability was determined by the MTT assay, as previously described.⁵⁵ Cell survival was normalized to untreated controls and is presented as a percentage.

Lymphoblasts from ALS and Control Individuals. Lymphocytes were obtained from blood samples of patients or healthy individuals (Table 5) after written informed consent. Patients were diagnosed as sporadic ALS according to El Escorial criteria⁵⁶ in the Doce de Octubre Hospital (Madrid, Spain).

All study protocols were approved by the Spanish Council of Higher Research Institutional Review Board and the Doce de Octubre Hospital and are in accordance with National and European Union Guidelines. Establishment of lymphoblastoid cell lines was performed in our laboratory as previously described by infecting peripheral blood lymphocytes with the Epstein–Barr virus.⁵⁷ Cells were grown in suspension in T-flasks in RPMI-1640 medium (Gibco, BRL) that contained 2 mM L-glutamine, 10% (v/v) fetal bovine serum (FBS), and 100 μ g/mL penicillin/streptomycin and were maintained in a humidified 5% CO₂ incubator at 37 °C. Lymphoblasts were seeded at an initial density of 1×10^6 mL⁻¹ in presence or absence of TTBK1 inhibitors (5 and 10 μ M) for 24 h. Then, cells were harvested and processed for Western blotting analysis.

Primary Rat Microglia Culture. Wistar rats were house held with free access to food and water and kept in a light–dark 12–12 h cycle. Experimental designs and procedures were in accordance to European Community and Italian laws and approved by the Ethical Committee for Animal Experimentation of the University of Bologna (protocol no. 17-72-1212).

Flasks used for cell cultures were previously covered with poly-L-lysine (10 μ g/mL) (Sigma-Aldrich, St. Louis, MO). Mixed cultures of glial cells were obtained from cerebral cortices of newborn rats as previously described.⁵⁸ Briefly, cerebral cortices were trypsinized and mechanically dissected after being cleared from meninges. The cell suspension was washed and resuspended in Basal Medium Eagle

(BME, Life Technologies Ltd, Paisley, UK) supplemented with 10% fetal bovine serum (FBS, Life Technologies), 50 mg/mL gentamicin, and 2 mM L-glutamine (Sigma-Aldrich). After six or seven days in culture, pure microglial cells were obtained through mechanical detachment, resuspended in serum-free BME, and plated on 35 mm diameter dishes at a density of 1.5×10^6 cells per 1.5 mL of medium per well. The medium was changed 30 min later in order to remove nonadhering cells. Cultures were maintained in standard conditions (5% CO₂ at 37 °C) and treated the day after being plated. Microglia cells were exposed to LPS (100 ng/mL) (Sigma-Aldrich) for 24 h. Compound 29 was added to the culture 1 h before the treatment with LPS at increasing concentrations (5 and 25 μM). Cells were collected for immunoblotting analysis.

Immunoblotting Analysis. Total protein extracts were obtained by lysing the cells and collecting them by centrifugation, as previously described.⁵⁹ Cytosolic and nuclear fractions were obtained using the Subcellular Protein Fractionation Kit (catalogue no. 78840, Thermo Fisher Scientific, Madrid, Spain) following the manufacturer's instructions. α-Tubulin and Lamin B1 were used as markers for cytosolic and nuclear fractions, respectively. Protein quantification was carried out using the Pierce BCA protein assay kit (Thermo-Fisher, Madrid Spain). Equal amounts of proteins were resolved by SDS-polyacrylamide gel electrophoresis. Proteins were then transferred to polyvinylidene fluoride (PVDF) membranes and immunodetected, as previously described. The primary antibodies used are listed in Table 5. Signals from the primary antibodies were amplified using species-specific antisera conjugated with horseradish peroxidase and detected with a chemiluminescent substrate detection system ECL (Bio-Rad, Alcobendas, Madrid, Spain). Relative band intensities were quantified using a ChemiDoc station with Quantity One 1D analysis software (Bio-Rad Laboratories, Madrid, Spain) and normalized using the intensities of GAPDH, α-tubulin, or Lamin B1.

Immunofluorescence. Cells were permeabilized for 10 min at RT with 0.25% Triton X-100 (Sigma-Aldrich), rinsed with PBS, and blocked with 2% BSA (Sigma-Aldrich) and 0.1% casein (Sigma-Aldrich) for 30 min at RT. After being fixed, cells were incubated with the TDP-43 monoclonal antibody (Table 5) in 6% BSA for 1 h at 37 °C, rinsed with PBS, and incubated with Alexa Fluor 488 antirabbit antibody (1:600, Jackson Immuno Research). HCS NuclearMask Deep Red (1:250, Thermo Fisher) was used to stain the cell nuclei. Finally, preparations were washed with 1% BSA and 0.1% casein and mounted onto fluoromount mounting medium (Sigma-Aldrich). Images were acquired for ~60 cells per group in $n = 3$ independent experiments using a confocal laser scanning microscope (CLMS) Leica TCS SPS with a 63× oil immersion objective. Quantification of TDP-43 was performed using ImageJ software.

Pharmacokinetic Studies. The study was conducted according to the guidelines of the Institutional Animal Ethics Committee (IAEC) and approved by Sai Life Sciences (Hinjewadi, Pune, India) (no. SAIDMPK/PK-21-03-262, March 2021). Healthy male BALB/c mice (8–12 weeks old) weighing between 17 and 30 g were used in the study. A total of 48 male mice were divided into two groups as group 1 ($n = 24$) and group 2 ($n = 24$) with a three mice per time point design. In both cases, the formulation was based in 90% of phosphate buffer saline (PBS, pH 7.4) with a 5% solutol HS-15 and 5% N-methyl-2-pyrrolidone at a dose of 5 or 10 mg/kg for i.p. or p.o. administration, respectively. Blood samples ($\approx 60 \mu\text{L}$) were collected from a set of three mice at each time point (0.08 (for i.p. only), 0.25, 0.5, 1, 2, 4, 6 (for p.o. only), 8, and 24 h). In addition, along with terminal blood samples, brain samples were collected at 0.08 (for i.p. only), 0.25, 0.5, 1, 2, 4, 6 (for p.o. only), 8, and 24 h post-dosing from three mice per time point. Immediately after the blood was collected, brain samples were collected from set of three animals for bioanalysis. Concentrations of the compound in mouse plasma and brain samples were determined by a fit-for-purpose LC–MS/MS method. The non-compartmental-analysis tool of Phoenix WinNonlin (ver. 8.0) was used to assess the pharmacokinetic parameters.

Animal Procedures, Treatment, and Sampling. A protocol authorized by the ethical committees of the regulatory institution and the UCM (ref PROEX 059/16) in agreement with regulations

(2010/63/EU) from the European Commission was in place for all the experiments done. Wild-type and Prp-hTDP-43(A31ST) transgenic littermate sibling mice were purchased from Jackson Laboratories (Bar Harbor, ME) and bred in house. Mice were maintained with food and water *ad libitum* in a temperature-controlled atmosphere (22 ± 1 °C) on a cycle of 12 h light–12 h dark. Genotyping of offspring were done as previously reported,³⁸ and four groups of male mice were randomly done ($n = 8$). Compound 29 was dissolved in 2.9% DMSO and Tween 80-saline buffer (1:16) and administered i.p. daily at a dose of 5 mg/kg. Control animals received vehicle injections. Treatment started at the age of 65 days old until animal sacrifice 30 days later. During all the treatments, physical appearance and animal weight gain were recorded. Spinal cords were rapidly collected and flash-frozen in 2-methylbutane cooled in dry ice and stored at –80 °C.

Tissue Slicing. Fixed spinal cords were sliced with a cryostat at the lumbar level (L4–L6) to obtain coronal sections (20 μm thick), which were collected on gelatin-coated slides. Sections were used for procedures of Nissl staining and immunofluorescence.

Nissl Staining. Slices were used for Nissl staining using cresyl violet, as previously described, which permitted the effects of each treatment on the cell number to be determined. A Leica DMRB microscope (Leica, Wetzlar, Germany) and a DFC300Fx camera (Leica) were used to study and photograph the tissue, respectively. To count the number of Nissl-stained motor neurons (>400 μm²) in the ventral horn, high-resolution photomicrographs were taken with a 10× objective under the same conditions of light, brightness, and contrast. Counting was carried out with ImageJ software (U.S. National Institutes of Health, Bethesda, Maryland; <http://imagej.nih.gov/ij/>, 1997–2012). At least six images per animal were analyzed to calculate the mean of each group ($n \geq 5$). Analyses were always conducted by experimenters who were blinded to genotype and treatment conditions. In all analyses, data were transformed to the percentage over the mean obtained in the wild-type group for each parameter.

Immunofluorescence Analysis. Spinal slices were used for the detection and quantification of Iba-1, GFAP, or ChAT immunofluorescence. After preincubation for 1 h with Tris-buffered saline with 0.1% Triton X-100 (pH 7.5), sections were sequentially incubated overnight at 4 °C with the following polyclonal antibodies: (i) anti-Iba-1 (Wako Chemicals, Richmond, VI) used at 1:500, (ii) anti-GFAP (Dako Cytomation, Glostrup, Denmark) used at 1:200, or (iii) ChAT (Merck Millipore, MA) used at 1:100. After incubation, sections were washed with Tris-buffered saline, and secondary antibodies were incubated for 2 h at 37 °C. For Iba-1 and GFAP staining, antirabbit secondary antibody conjugated with Alexa 488 (Invitrogen, Carlsbad, CA) was used at 1:200. For ChAT staining, antigoat secondary antibody conjugated with Alexa 546 (Invitrogen, ThermoFisher Scientific, MA) was used. Sections were then washed and mounted with the Faramount aqueous mounting medium (Dako Cytomation, Glostrup, Denmark). A DMRB microscope and a DFC300Fx camera (Leica, Wetzlar, Germany) were used for slide observation and photography, respectively. The mean density of immunolabeling was measured in the selected areas with ImageJ software (NIH). At least six images per animal were analyzed to calculate the mean of each group ($n \geq 5$). Again, all data were transformed to the percentage over the mean obtained in the wild-type group for each parameter.

Statistical Analysis. Statistical analyses were performed with Graph Pad Prism ver. 9. All the statistical data are presented as the mean ± standard error of the mean (SEM). Normality was checked with the Shapiro–Wilk test. Parametric tests were therefore used in the statistical analysis. Significant differences between groups were evaluated by using Student's *t*-test or by analysis of variance (ANOVA), followed by the Fisher's LSD test for multiple comparisons. A value of $p < 0.05$ was considered significant.

■ ASSOCIATED CONTENT

SI Supporting Information

The Supporting Information is available free of charge at <https://pubs.acs.org/doi/10.1021/acs.jmedchem.1c01942>.

Data collection, refinement statistics, crystal structures, MM-GBSA parameters, experimental permeability data, antibodies used in WB and immunohistochemistry analyses, viability studies for TTBK1 inhibitors, neuroprotection of TTBK1 inhibitors, images of the immunomodulatory effect of compound 29, HPLC-MS chromatograms of lead compounds ([PDF](#))

Molecular formula strings ([CSV](#))

■ AUTHOR INFORMATION

Corresponding Author

Ana Martínez — Centro de Investigaciones Biológicas Margarita Salas—CSIC, 28040 Madrid, Spain; Centro de Investigación Biomédica en Red de Enfermedades Neurodegenerativas (CIBERNED), Instituto de Salud Carlos III, 28031 Madrid, Spain; [orcid.org/0000-0002-2707-8110](#); Email: ana.martinez@csic.es

Authors

Vanesa Nozal — Centro de Investigaciones Biológicas Margarita Salas—CSIC, 28040 Madrid, Spain; Centro de Investigación Biomédica en Red de Enfermedades Neurodegenerativas (CIBERNED), Instituto de Salud Carlos III, 28031 Madrid, Spain

Loreto Martínez-González — Centro de Investigaciones Biológicas Margarita Salas—CSIC, 28040 Madrid, Spain; Centro de Investigación Biomédica en Red de Enfermedades Neurodegenerativas (CIBERNED), Instituto de Salud Carlos III, 28031 Madrid, Spain

Marta Gómez-Almería — Instituto de Investigación en Neuroquímica, Departamento de Bioquímica y Biología Molecular, Facultad de Medicina, Universidad Complutense de Madrid, 28040 Madrid, Spain

Claudia Gonzalo-Consuegra — Instituto de Investigación en Neuroquímica, Departamento de Bioquímica y Biología Molecular, Facultad de Medicina, Universidad Complutense de Madrid, 28040 Madrid, Spain

Paula Santana — Facultad de Ingeniería, Instituto de Ciencias Químicas Aplicadas, Universidad Autónoma de Chile el Llano Subercaseaux, 2801 San Miguel, Santiago, Chile

Apirat Chaikud — Institute for Pharmaceutical Chemistry, Goethe University Frankfurt, 60438 Frankfurt, Germany; Structural Genomics Consortium, Buchmann Institute for Life Sciences, Goethe University Frankfurt, 60438 Frankfurt, Germany; [orcid.org/0000-0003-1120-2209](#)

Eva Pérez-Cuevas — Centro de Investigaciones Biológicas Margarita Salas—CSIC, 28040 Madrid, Spain; Centro de Investigación Biomédica en Red de Enfermedades Neurodegenerativas (CIBERNED), Instituto de Salud Carlos III, 28031 Madrid, Spain

Stefan Knapp — Institute for Pharmaceutical Chemistry, Goethe University Frankfurt, 60438 Frankfurt, Germany; Structural Genomics Consortium, Buchmann Institute for Life Sciences, Goethe University Frankfurt, 60438 Frankfurt, Germany; [orcid.org/0000-0001-5995-6494](#)

Daniel Lietha — Centro de Investigaciones Biológicas Margarita Salas—CSIC, 28040 Madrid, Spain

David Ramírez — Departamento de Farmacología, Facultad de Ciencias Biológicas, Universidad de Concepción, 1290 Concepción, Chile

Sabrina Petralla — Department of Pharmacy and Biotechnology, University of Bologna, 40126 Bologna, Italy
Barbara Monti — Department of Pharmacy and Biotechnology, University of Bologna, 40126 Bologna, Italy; [orcid.org/0000-0003-0330-482X](#)

Carmen Gil — Centro de Investigaciones Biológicas Margarita Salas—CSIC, 28040 Madrid, Spain; [orcid.org/0000-0002-3882-6081](#)

Angeles Martín-Requero — Centro de Investigaciones Biológicas Margarita Salas—CSIC, 28040 Madrid, Spain; Centro de Investigación Biomédica en Red de Enfermedades Neurodegenerativas (CIBERNED), Instituto de Salud Carlos III, 28031 Madrid, Spain

Valle Palomo — Centro de Investigaciones Biológicas Margarita Salas—CSIC, 28040 Madrid, Spain; Centro de Investigación Biomédica en Red de Enfermedades Neurodegenerativas (CIBERNED), Instituto de Salud Carlos III, 28031 Madrid, Spain

Eva de Lago — Centro de Investigación Biomédica en Red de Enfermedades Neurodegenerativas (CIBERNED), Instituto de Salud Carlos III, 28031 Madrid, Spain; Instituto de Investigación en Neuroquímica, Departamento de Bioquímica y Biología Molecular, Facultad de Medicina, Universidad Complutense de Madrid, 28040 Madrid, Spain

Complete contact information is available at:
<https://pubs.acs.org/10.1021/acs.jmedchem.1c01942>

Notes

The authors declare no competing financial interest.

■ ACKNOWLEDGMENTS

This work was supported by Comunidad de Madrid (grant B2017/BMD-3813), the European Social Fund+ (ESF+), MINECO (Grants SAF2016-76693-R to A.M., RTI2018-098885-B-I00 to E.d.L., and CTQ2015-66313-R to A.M.R.), AIE (RTI2018-099318-B-I00 to D.L., cofunded by the European Regional Development Fund (FEDER)), ISCiii CIBERNED (CB18/05/00040 to A.M., V.P., and A.M.R. and CB06/05/0089 to E.d.L.), MECD (FPU16/04466 to V.N.), Cost Action CA15135 “MuTaLig” (COST-STSM-CA15135-37514 to L.M.G.), FONDECYT (Grant 11180604 to D.R.). V.P. has received financial support through the Postdoctoral Junior Leader Fellowship Program (LCF/BQ/PR18/11640007) from “la Caixa” Banking Foundation. This work has been awarded by the SEQT (Spanish Society of Medicinal Chemistry) for young researchers in their XX edition. We thank the staff at the ALBA synchrotron facilities for their assistance during the X-ray diffraction data collection and Pilar López Navajas for help during TTBK1 protein purification.

■ ABBREVIATIONS USED

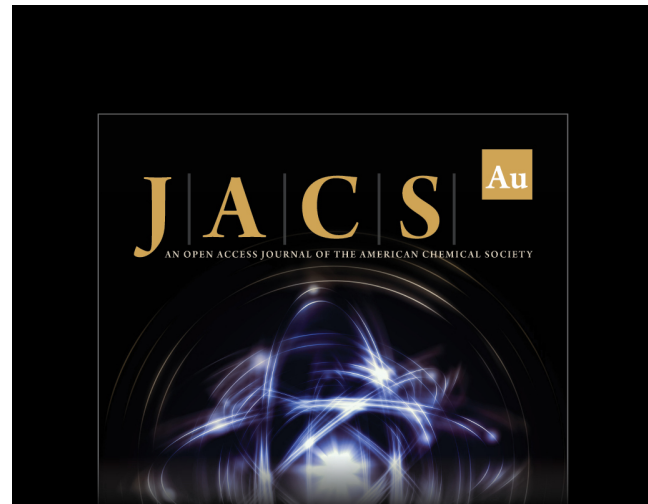
AD, Alzheimer’s disease; ALS, amyotrophic lateral sclerosis; BBB, blood–brain barrier; CNS, central nervous system; EA, ethacrynic acid; FTD-TDP, frontotemporal dementia with TDP-43 aggregates; LATE, limbic-predominant age-related TDP-43 encephalopathy; LPS, lipopolysaccharide; MM-GBSA, molecular mechanics-generalized Born surface area; iNOS, inducible nitric oxide synthase; OA, okadaic acid; PAMPA, parallel artificial membranes permeability assay; RMSD, root-

mean-square deviation; TDP-43, transactive response DNA binding protein of 43 kDa; TREM2, triggering receptor expressed on myeloid cells 2; TTBK1, τ -tubulin kinase 1; TTBK2, Tau-tubulin kinase 2.

■ REFERENCES

- (1) Scotter, E. L.; Chen, H. J.; Shaw, C. E. TDP-43 proteinopathy and ALS: Insights into disease mechanisms and therapeutic targets. *Neurotherapeutics* **2015**, *12*, 352–363.
- (2) Weskamp, K.; Barmada, S. J. TDP43 and RNA instability in amyotrophic lateral sclerosis. *Brain Res.* **2018**, *1693*, 67–74.
- (3) de Boer, E. M. J.; Orie, V. K.; Williams, T.; Baker, M. R.; De Oliveira, H. M.; Polvikoski, T.; Silsby, M.; Menon, P.; van den Bos, M.; Halliday, G. M.; van den Berg, L. H.; Van Den Bosch, L.; van Damme, P.; Kiernan, M. C.; van Es, M. A.; Vucic, S. TDP-43 proteinopathies: a new wave of neurodegenerative diseases. *J. Neurol Neurosurg Psychiatry* **2021**, *92*, 86–95.
- (4) Suk, T. R.; Rousseaux, M. W. C. The role of TDP-43 mislocalization in amyotrophic lateral sclerosis. *Mol. Neurodegener* **2020**, *15*, 45.
- (5) Prasad, A.; Bharathi, V.; Sivalingam, V.; Girdhar, A.; Patel, B. K. Molecular mechanisms of TDP-43 misfolding and pathology in amyotrophic lateral sclerosis. *Front Mol. Neurosci* **2019**, *12*, 25.
- (6) Palomo, V.; Tosat-Bitrian, C.; Nozal, V.; Nagaraj, S.; Martin-Requero, A.; Martinez, A. TDP-43: A key therapeutic target beyond amyotrophic lateral sclerosis. *ACS Chem. Neurosci.* **2019**, *10*, 1183–1196.
- (7) Moujalled, D.; James, J. L.; Parker, S. J.; Lidgerwood, G. E.; Duncan, C.; Meyerowitz, J.; Nonaka, T.; Hasegawa, M.; Kanninen, K. M.; Grubman, A.; Liddell, J. R.; Crouch, P. J.; White, A. R. Kinase inhibitor screening identifies cyclin-dependent kinases and glycogen synthase kinase 3 as potential modulators of TDP-43 cytosolic accumulation during cell stress. *PLoS One* **2013**, *8*, e67433.
- (8) Kametani, F.; Nonaka, T.; Suzuki, T.; Arai, T.; Dohmae, N.; Akiyama, H.; Hasegawa, M. Identification of casein kinase-1 phosphorylation sites on TDP-43. *Biochem. Biophys. Res. Commun.* **2009**, *382*, 405–409.
- (9) Liachko, N. F.; McMillan, P. J.; Guthrie, C. R.; Bird, T. D.; Leverenz, J. B.; Kraemer, B. C. CDC7 inhibition blocks pathological TDP-43 phosphorylation and neurodegeneration. *Ann. Neurol.* **2013**, *74*, 39–52.
- (10) Li, W.; Reeb, A. N.; Lin, B.; Subramanian, P.; Fey, E. E.; Knoverek, C. R.; French, R. L.; Bigio, E. H.; Ayala, Y. M. Heat shock-induced phosphorylation of TAR DNA-binding protein 43 (TDP-43) by MAPK/ERK kinase regulates TDP-43 function. *J. Biol. Chem.* **2017**, *292*, 5089–5100.
- (11) Liachko, N. F.; McMillan, P. J.; Strovas, T. J.; Loomis, E.; Greenup, L.; Murrell, J. R.; Ghetti, B.; Raskind, M. A.; Montine, T. J.; Bird, T. D.; Leverenz, J. B.; Kraemer, B. C. The tau tubulin kinases TTBK1/2 promote accumulation of pathological TDP-43. *PLoS Genet* **2014**, *10*, e1004803.
- (12) Palomo, V.; Nozal, V.; Rojas-Prats, E.; Gil, C.; Martinez, A. Protein kinase inhibitors for amyotrophic lateral sclerosis therapy. *Br. J. Pharmacol.* **2021**, *178*, 1316–1335.
- (13) Martinez-Gonzalez, L.; Gonzalo-Consuerga, C.; Gomez-Almeria, M.; Porras, G.; de Lago, E.; Martin-Requero, A.; Martinez, A. Tideglusib, a non-ATP competitive inhibitor of GSK-3beta as a drug candidate for the treatment of amyotrophic lateral sclerosis. *Int. J. Mol. Sci.* **2021**, *22*, 8975–8989.
- (14) Martinez-Gonzalez, L.; Rodriguez-Cueto, C.; Cabezudo, D.; Bartolome, F.; Andres-Benito, P.; Ferrer, I.; Gil, C.; Martin-Requero, A.; Fernandez-Ruiz, J.; Martinez, A.; de Lago, E. Motor neuron preservation and decrease of in vivo TDP-43 phosphorylation by protein CK-1delta kinase inhibitor treatment. *Sci. Rep.* **2020**, *10*, 4449.
- (15) Rojas-Prats, E.; Martinez-Gonzalez, L.; Gonzalo-Consuerga, C.; Liachko, N. F.; Perez, C.; Ramirez, D.; Kraemer, B. C.; Martin-Requero, A.; Perez, D. I.; Gil, C.; de Lago, E.; Martinez, A. Targeting nuclear protein TDP-43 by cell division cycle kinase 7 inhibitors: A new therapeutic approach for amyotrophic lateral sclerosis. *Eur. J. Med. Chem.* **2021**, *210*, 112968.
- (16) Halkina, T.; Henderson, J. L.; Lin, E. Y.; Himmelbauer, M. K.; Jones, J. H.; Nevalainen, M.; Feng, J.; King, K.; Rooney, M.; Johnson, J. L.; Marcotte, D. J.; Chodaparambil, J. V.; Kumar, P. R.; Patterson, T. A.; Murugan, P.; Schuman, E.; Wong, L.; Hesson, T.; Lamore, S.; Bao, C.; Calhoun, M.; Certo, H.; Amaral, B.; Dillon, G. M.; Gilfillan, R.; de Turiso, F. G. Discovery of potent and brain-penetrant tau tubulin kinase 1 (TTBK1) inhibitors that lower tau phosphorylation in vivo. *J. Med. Chem.* **2021**, *64*, 6358–6380.
- (17) Jackson, P. K. TTBK2 kinase: Linking primary cilia and cerebellar ataxias. *Cell* **2012**, *151*, 697–699.
- (18) Cajanek, L.; Nigg, E. A. Cep164 triggers ciliogenesis by recruiting tau tubulin kinase 2 to the mother centriole. *Proc. Natl. Acad. Sci. U. S. A.* **2014**, *111*, E2841.
- (19) Taylor, L. M.; McMillan, P. J.; Kraemer, B. C.; Liachko, N. F. Tau tubulin kinases in proteinopathy. *FEBS J.* **2019**, *286*, 2434–2446.
- (20) Sato, S.; Cerny, R. L.; Buescher, J. L.; Ikezu, T. Tau-tubulin kinase 1 (TTBK1), a neuron-specific tau kinase candidate, is involved in tau phosphorylation and aggregation. *J. Neurochem.* **2006**, *98*, 1573–1584.
- (21) Lund, H.; Cowburn, R. F.; Gustafsson, E.; Stromberg, K.; Svensson, A.; Dahllund, L.; Malinowsky, D.; Sunnemark, D. Tau-tubulin kinase 1 expression, phosphorylation and co-localization with phospho-Ser422 tau in the Alzheimer's disease brain. *Brain Pathol* **2013**, *23*, 378–389.
- (22) Bao, C.; Bajrami, B.; Marcotte, D. J.; Chodaparambil, J. V.; Kerns, H. M.; Henderson, J.; Wei, R.; Gao, B.; Dillon, G. M. Mechanisms of regulation and diverse activities of tau-tubulin kinase (TTBK) isoforms. *Cell Mol. Neurobiol* **2021**, *41*, 669–685.
- (23) Nozal, V.; Martinez, A. Tau tubulin kinase 1 (TTBK1), a new player in the fight against neurodegenerative diseases. *Eur. J. Med. Chem.* **2019**, *161*, 39.
- (24) Xue, Y.; Wan, P. T.; Hillertz, P.; Schweikart, F.; Zhao, Y.; Wissler, L.; Dekker, N. X-ray structural analysis of tau-tubulin kinase 1 and its interactions with small molecular inhibitors. *ChemMedChem* **2013**, *8*, 1846–1854.
- (25) Kiefer, S. E.; Chang, C. J.; Kimura, S. R.; Gao, M.; Xie, D.; Zhang, Y.; Zhang, G.; Gill, M. B.; Mastalerz, H.; Thompson, L. A.; Cacace, A. M.; Sheriff, S. The structure of human tau-tubulin kinase 1 both in the apo form and in complex with an inhibitor. *Acta Crystallogr. F Struct Biol. Commun.* **2014**, *70*, 173–181.
- (26) Dillon, G. M.; Henderson, J. L.; Bao, C.; Joyce, J. A.; Calhoun, M.; Amaral, B.; King, K. W.; Bajrami, B.; Rabah, D. Acute inhibition of the CNS-specific kinase TTBK1 significantly lowers tau phosphorylation at several disease relevant sites. *PLoS One* **2020**, *15*, e0228771.
- (27) Marcotte, D. J.; Spilker, K. A.; Wen, D.; Hesson, T.; Patterson, T. A.; Kumar, P. R.; Chodaparambil, J. V. The crystal structure of the catalytic domain of tau tubulin kinase 2 in complex with a small-molecule inhibitor. *Acta Crystallogr. F Struct Biol. Commun.* **2020**, *76*, 103–108.
- (28) Attwood, M. M.; Fabbro, D.; Sokolov, A. V.; Knapp, S.; Schiott, H. B. Trends in kinase drug discovery: Targets, indications and inhibitor design. *Nat. Rev. Drug Discov* **2021**, *20*, 839–861.
- (29) Staderini, M.; Bolognesi, M. L.; Menéndez, J. C. Lewis acid-catalyzed generation of C-C and C-N bonds on π -deficient heterocyclic substrates. *Adv. Synth Catal* **2015**, *357*, 185–195.
- (30) Kolb, H. C.; Finn, M. G.; Sharpless, K. B. Click chemistry: Diverse chemical function from a few good reactions. *Angew. Chem., Int. Ed. Engl.* **2001**, *40*, 2004–2021.
- (31) Young, M. A.; Shah, N. P.; Chao, L. H.; Seeliger, M.; Milanov, Z. V.; Biggs, W. H., 3rd; Treiber, D. K.; Patel, H. K.; Zarrinkar, P. P.; Lockhart, D. J.; Sawyers, C. L.; Kuriyan, J. Structure of the kinase domain of an imatinib-resistant Abl mutant in complex with the Aurora kinase inhibitor VX-680. *Cancer Res.* **2006**, *66*, 1007–1014.
- (32) Schroder, M.; Bullock, A. N.; Fedorov, O.; Bracher, F.; Chaikuad, A.; Knapp, S. DFG-1 residue controls inhibitor binding

- mode and affinity, providing a basis for rational design of kinase inhibitor selectivity. *J. Med. Chem.* **2020**, *63*, 10224–10234.
- (33) Cheng, A. C.; Eksterowicz, J.; Geuns-Meyer, S.; Sun, Y. Analysis of kinase inhibitor selectivity using a thermodynamics-based partition index. *J. Med. Chem.* **2010**, *53*, 4502–4510.
- (34) Iguchi, Y.; Katsuno, M.; Takagi, S.; Ishigaki, S.; Niwa, J.; Hasegawa, M.; Tanaka, F.; Sobue, G. Oxidative stress induced by glutathione depletion reproduces pathological modifications of TDP-43 linked to TDP-43 proteinopathies. *Neurobiol Dis* **2012**, *45*, 862–870.
- (35) Boban, M.; Babic Leko, M.; Miskic, T.; Hof, P. R.; Simic, G. Human neuroblastoma SH-SY5Y cells treated with okadaic acid express phosphorylated high molecular weight tau-immunoreactive protein species. *J. Neurosci Methods* **2019**, *319*, 60–68.
- (36) Haukedal, H.; Freude, K. Implications of microglia in amyotrophic lateral sclerosis and frontotemporal dementia. *J. Mol. Biol.* **2019**, *431*, 1818–1829.
- (37) Tang, Y.; Le, W. Differential roles of M1 and M2 microglia in neurodegenerative diseases. *Mol. Neurobiol* **2016**, *53*, 1181–1194.
- (38) Węgorzewska, I.; Bell, S.; Cairns, N. J.; Miller, T. M.; Baloh, R. H. TDP-43 mutant transgenic mice develop features of ALS and frontotemporal lobar degeneration. *Proc. Natl. Acad. Sci. U. S. A.* **2009**, *106*, 18809–18814.
- (39) Poso, D.; Martinez-Gonzalez, L.; Bartolome, F.; Nagaraj, S.; Porras, G.; Martinez, A.; Martin-Requero, A. Recapitulation of pathological TDP-43 features in immortalized lymphocytes from sporadic ALS patients. *Mol. Neurobiol* **2019**, *56*, 2424–2432.
- (40) Arnold, L. A.; Moyer, M. P.; Sobolov-Jaynes, S. B. Heterocyclic ring-fused pyrimidine derivatives. US 6395733 B1, 1995.
- (41) Kabsch, W. Integration, scaling, space-group assignment and post-refinement. *Acta Crystallogr. D Biol. Crystallogr.* **2010**, *66*, 133–144.
- (42) Evans, P. R.; Murshudov, G. N. How good are my data and what is the resolution? *Acta Crystallogr. D Biol. Crystallogr.* **2013**, *69*, 1204–1214.
- (43) McCoy, A. J.; Grosse-Kunstleve, R. W.; Adams, P. D.; Winn, M. D.; Storoni, L. C.; Read, R. J. Phaser crystallographic software. *J. Appl. Crystallogr.* **2007**, *40*, 658–674.
- (44) Murshudov, G. N.; Vagin, A. A.; Dodson, E. J. Refinement of macromolecular structures by the maximum-likelihood method. *Acta Crystallogr. D Biol. Crystallogr.* **1997**, *53*, 240–255.
- (45) Emsley, P.; Cowtan, K. Coot: Model-building tools for molecular graphics. *Acta Crystallogr. D Biol. Crystallogr.* **2004**, *60*, 2126–2132.
- (46) Halgren, T. A.; Murphy, R. B.; Friesner, R. A.; Beard, H. S.; Frye, L. L.; Pollard, W. T.; Banks, J. L. Glide: A new approach for rapid, accurate docking and scoring. 2. Enrichment factors in database screening. *J. Med. Chem.* **2004**, *47*, 1750–1759.
- (47) Friesner, R. A.; Banks, J. L.; Murphy, R. B.; Halgren, T. A.; Klicic, J. J.; Mainz, D. T.; Repasky, M. P.; Knoll, E. H.; Shelley, M.; Perry, J. K.; Shaw, D. E.; Francis, P.; Shenkin, P. S. Glide: A new approach for rapid, accurate docking and scoring. 1. Method and assessment of docking accuracy. *J. Med. Chem.* **2004**, *47*, 1739–1749.
- (48) Sastry, G. M.; Adzhigirey, M.; Day, T.; Annabhimmoju, R.; Sherman, W. Protein and ligand preparation: Parameters, protocols, and influence on virtual screening enrichments. *J. Comput. Aided Mol. Des* **2013**, *27*, 221–234.
- (49) Friesner, R. A.; Murphy, R. B.; Repasky, M. P.; Frye, L. L.; Greenwood, J. R.; Halgren, T. A.; Sanschagrin, P. C.; Mainz, D. T. Extra precision glide: docking and scoring incorporating a model of hydrophobic enclosure for protein-ligand complexes. *J. Med. Chem.* **2006**, *49*, 6177–6196.
- (50) Bowers, K. J.; Chow, E.; Xu, H.; Dror, R. O.; Eastwood, M. P.; Gregersen, B. A.; Klepeis, J. L.; Kolossvary, I.; Moraes, M. A.; Sacerdoti, F. D.; Salmon, J. K.; Shan, Y.; Shaw, D. E. Scalable algorithms for molecular dynamics simulations on commodity clusters. *SC 2006 Proceedings Supercomputing 2006* **2006**, *43*.
- (51) Roos, K.; Wu, C.; Damm, W.; Reboul, M.; Stevenson, J. M.; Lu, C.; Dahlgren, M. K.; Mondal, S.; Chen, W.; Wang, L.; Abel, R.; Friesner, R. A.; Harder, E. D. OPLS3e: Extending force field coverage for drug-like small molecules. *J. Chem. Theory Comput.* **2019**, *15*, 1863–1874.
- (52) Martyna, G. J.; Tobias, D. J.; Klein, M. L. Constant pressure molecular dynamics algorithms. *J. Chem. Phys.* **1994**, *101*, 4177–4189.
- (53) Bain, J.; Plater, L.; Elliott, M.; Shpiro, N.; Hastie, C. J.; McLauchlan, H.; Klevernic, I.; Arthur, J. S.; Alessi, D. R.; Cohen, P. The selectivity of protein kinase inhibitors: a further update. *Biochem. J.* **2007**, *408*, 297–315.
- (54) Di, L.; Kerns, E. H.; Fan, K.; McConnell, O. J.; Carter, G. T. High throughput artificial membrane permeability assay for blood-brain barrier. *Eur. J. Med. Chem.* **2003**, *38*, 223–232.
- (55) Morgan, D. M. Tetrazolium (MTT) assay for cellular viability and activity. *Methods Mol. Biol.* **1997**, *79*, 179–183.
- (56) Agosta, F.; Al-Chalabi, A.; Filippi, M.; Hardiman, O.; Kaji, R.; Meininguer, V.; Nakano, I.; Shaw, P.; Shefner, J.; van den Berg, L. H.; Ludolph, A. The El Escorial criteria: Strengths and weaknesses. *Amyotroph Lateral Sclerosis Frontotemporal Degeneration* **2015**, *16*, 1.
- (57) Omi, N.; Tokuda, Y.; Ikeda, Y.; Ueno, M.; Mori, K.; Sotozono, C.; Kinoshita, S.; Nakano, M.; Tashiro, K. Efficient and reliable establishment of lymphoblastoid cell lines by Epstein-Barr virus transformation from a limited amount of peripheral blood. *Sci. Rep.* **2017**, *7*, 43833.
- (58) Polazzi, E.; Gianni, T.; Contestabile, A. Microglial cells protect cerebellar granule neurons from apoptosis: Evidence for reciprocal signaling. *Glia* **2001**, *36*, 271–280.
- (59) Alquezar, C.; Salado, I. G.; de la Encarnacion, A.; Perez, D. I.; Moreno, F.; Gil, C.; de Munain, A. L.; Martinez, A.; Martin-Requero, A. Targeting TDP-43 phosphorylation by casein kinase-1 δ inhibitors: a novel strategy for the treatment of frontotemporal dementia. *Mol. Neurodegener* **2016**, *11*, 36.



JA|C|S
AN OPEN ACCESS JOURNAL OF THE AMERICAN CHEMICAL SOCIETY

 Editor-in-Chief
Prof. Christopher W. Jones
Georgia Institute of Technology, USA

Open for Submissions 

pubs.acs.org/jacsau ACS Publications
Most Trusted. Most Cited. Most Read.